Quasi-periodic frequency analysis using averaging-extrapolation methods*

Alejandro Luque†
Departament de Matemàtica Aplicada i Anàlisi
Universitat de Barcelona
Gran Via 585, 08007 Barcelona (Spain).

Jordi Villanueva‡
Departament de Matemàtica Aplicada I,
Universitat Politècnica de Catalunya,
Diagonal 647, 08028 Barcelona (Spain).

May 6, 2013

Abstract

We present a new approach to numerically compute the basic frequencies of a quasi-periodic signal. Although a complete toolkit for frequency analysis is presented, this methodology is better understood as a refinement process for any of the frequencies, provided we have a rough approximation of it. The cornerstone of this work is a recently developed methodology for the computation of Diophantine rotation numbers of circle diffeomorphisms, which is based on suitable averages of the iterates and Richardson extrapolation. This methodology was successfully extended later to deal with rotation numbers of quasi-periodic invariant curves of planar maps. In this paper, we address the case of a signal with an arbitrary number of frequencies. The most outstanding aspect of our approach is that frequencies can be calculated, with high accuracy at a moderate computational cost, without simultaneously computing the Fourier representation of the signal. The method consists in constructing a new quasi-periodic signal by appropriate averages of phase-shifted iterates of the original one. This allows us to define a quasi-periodic orbit on the circle in such a way that the frequency to be computed leads the rotation of the iterates. This orbit is well-suited for the application of the aforementioned averaging-extrapolation methodology for computing rotation numbers. We illustrate the presented methodology with the study of the vicinity of the Lagrangian equilibrium points of the Restricted Three Body Problem and we consider the effect of additional planets using a multicircular model.

*This work has been partially supported by the Spanish MINECO-FEDER grants MTM2009-06973, MTM2012-31714, MTM2012-32541 and the Catalan CUR-DIUE grant 2009SGR859. Moreover, the research of A. L. has been supported by the *Juan de la Cierva* fellow JCI-2010-06517.

†luque@maia.ub.es
‡jordi.villanueva@upc.edu

Contents

1 Introduction

Invariant tori play a fundamental role in the understanding of the long-term behaviour of dynamical systems. This is mainly true for Hamiltonian systems —and also for exact symplectic maps, their discrete counterpart. If the Hamiltonian function is a small perturbation of an integrable one, KAM Theorem claims that, under generic assumptions, there is plenty of (maximal dimensional) invariant tori carrying quasi-periodic motion [1]. Invariant tori are also present far from integrability, in the sense that they persist for larger values of the perturbation than the predicted by KAM theory. Beyond this fact, there are other ways to generate quasi-periodic solutions apart from the close-to-integrable context. For example, if a system is forced periodically or quasi-periodically, then fixed points, periodic orbits and invariant tori capture the frequencies of the perturbation [23, 38]. An analogous phenomenon takes place in the autonomous case, in connection with the excitation of elliptic normal modes of linearly stable fixed points, periodic orbits or lower dimensional invariant tori [10, 22]. These small oscillations generate new invariant tori. In addition, invariant tori are effective barriers to diffusion in phase space, in the sense that trajectories close to a maximal dimensional torus or to a linearly stable lower dimensional one, remain around it for a very long time [22, 33] (i. e., invariant tori are very "sticky"). These considerations lead quasi-periodic solutions to be the fundamental class of "stable solutions" in the Hamiltonian context. These solutions are relevant in applications to Celestial Mechanics, Astrodynamics, Molecular Dynamics or Plasma-Beam Physics. Of course, beyond the study of Hamiltonian systems and symplectic maps, existence of quasi-periodic solutions with stable behaviour also occurs in other contexts, such as in dissipative ordinary differential equations [3]. We refer the interested reader to [3, 4, 6, 38] and references therein for a wider picture of quasi-periodicity in dynamical systems.

Given an initial condition on a quasi-periodic torus, we can reconstruct this object from the corresponding orbit. If the dynamical system is defined by a map (discrete case), the iteration of this initial condition under the map naturally defines a quasi-periodic signal. If the dynamical system is defined by a vector field (continuous case), this signal is obtained by numerical integration of the initial condition and defining either a stroboscopic or a Poincaré section (see remarks 2.7 and 2.8 for a more detailed discussion). The crucial issue to characterize quasi-periodic signals is to compute their frequencies. Indeed, the evolution of these frequencies along a family of trajectories allows us to understand the global behavior of the system, for example, by detecting resonances through the analysis of ratios between the computed frequencies. In addition, the regularity of the frequency map also provides information on the persistence of invariant tori. Moreover, the variation of the (local) frequencies with time is a dynamical indicator to measure diffusion and chaos [25].

The computation of frequencies and amplitudes of a given signal is called quasi-periodic frequency analysis. We note that frequencies define a dense set of $\mathbb{R}$, although only a finite number of them may be independent. We refer as vector of basic frequencies to any collection of independent frequencies. Typically, frequencies are approximated by the peaks of the Discrete Fourier Transform (DFT) associated to a sample of points of the signal (see (31)). The size of the peak gives an approximation to the corresponding amplitude. This approximation is good up to errors of order $1/N$, where N is the number of points of the truncated signal. An important source of error is a phenomenon known as leakage. For periodic functions (the quasi-periodic case is similar), when the length T of the time interval spanned by the sample is not an integer multiple of the period of the function (or equivalently, when the frequency of the function is not an integer multiple of the "frequency" $1/T$ associated to the sample interval $[0, T]$), there appear in the DFT spurious frequencies and the peaks are displaced. A procedure based on refined Fourier techniques to reduce leakage and improve this approximation was introduced in [25] (see also [26, 28]). This celebrated methodology introduces in the definition of the DFT a suitable window function, usually a power $p \geq 1$ of the so-called Hanning filter. After multiplying the quasi-periodic function by this window function, the derivatives of the new function vanish (up to order $2p - 1$) at the endpoints of the interval. If the quasi-periodic function is smooth enough, then this new function can be extended outside $[0, T]$ as a periodic function of class $\mathcal{C}^{2p-1}$. This regularization has the effect of reducing the leakage phenomenon and allows improving the resolution of the peaks corresponding to the dominant frequencies. After a frequency and its amplitude have been determined, this harmonic can be subtracted from the original signal, thus improving the computation of the remaining frequencies. This methodology has been successfully applied to a wide set of problems (see for example [12, 27, 35] and references therein).

Among the improvements of this methodology, we highlight [13, 14]. The cornerstone of these papers is to refine both frequencies and amplitudes by means of a collocation method. Specifically, the signal is fitted to a generic Fourier expansion. After truncation of the series and discretization of the signal to a finite sample, the resulting system of nonlinear equations is solved simultaneously for both the frequencies and the Fourier coefficients (using the Newton method). The approximations of frequencies and amplitudes provided by the DFT are used as the initial guess for the solution of these equations.

There are other approaches to frequency analysis in the literature. For example, in [41] a method based on wavelets is presented, while [18] relies on the construction of sequences of orthogonal polynomials (frequencies are approximated by the zeros of these polynomials).

The methodology developed in the present paper assumes that we have a finite number of iterates of a quasi-periodic signal with Diophantine frequencies. We also suppose that the signal is analytic, although large enough differentiability suffices. Before discussing our approach to frequency analysis, let us outline some previous works that have motivated it.

The cornerstone of our construction is a method introduced in [36] for computing Diophantine rotation numbers of circle diffeomorphisms. This method was justified under the assumption that the map is conjugate to a rigid rotation in a sufficiently smooth way. Basically, it consists in averaging the iterates of the map (actually its lift), together with Richardson extrapolation. In most of the cases, it is capable of computing the rotation number with high accuracy at low cost. We refer to [8, 29, 37] for some works where this approach has been useful to deal with problems related to circle maps.

The method of [36] was successfully extended in [30] to compute rotation numbers of quasi-periodic invariant curves of planar maps and, more in general, of quasi-periodic signals with one frequency ω. The methodology consists in building a new quasi-periodic signal having the same frequency. Any new iterate is defined by a weighted average of L consecutive phase-shifted iterates of the signal. Shifts are defined in terms of an approximation to the frequency of the signal (information on the amplitudes is not required). The purpose of these averages is to remove the main folds of the planar curve described by the signal, so that the new one resembles as closely as possible a circle centered at the origin. For this reason, the construction is referred as "unfolding process". The target is that the projection of the new signal onto the unit circle induces a circle diffeomorphism, defined by means of the correspondence between consecutive iterates. The rotation number of this map, which coincides with the frequency of the curve, can be obtained by the method of [36].

To ensure that the projection of the iterates generates a circle map, we can ask the unfolded curve to be a graph over the argument. From the theoretical viewpoint, this achievement is possible if one has a sufficiently good approximation of the frequency and L is large enough. However, the complete unfolding of the signal can be quite expensive. It turns out that the convergence of the curve to a circle can be accelerated by means of higher order averages and extrapolation (in analogy to the methodology of [36] for computing the rotation number). Still, if the original curve is very intricate, it will be very hard to obtain a graph even using this refined approach. Fortunately, in practice this methodology works under weaker conditions. It suffices to unfold the curve in such a way that the frequency ω leads the rotation of the new iterates around the origin (i. e., $\omega/2\pi$ is the averaged number of turns by iterate). This is achieved under a less expensive computational cost. Roughly speaking, this assumption means that we remove only the main folds of the signal and that the size of the remaining ones is small compared with the frequency. Although the projection of the iterates onto the circle does not define a circle map, in general it defines a smooth quasi-periodic signal on the circle, rotating with frequency ω. It turns out that the method of [36] also works in this case. The reason is that the key ingredient in [36] is not that the map is conjugate to a rigid rotation, but that the iterates behave quasi-periodically on the circle. Hence, beyond circle maps, the construction of [36] works for the computation of the leading frequency of an arbitrary quasi-periodic signal on the circle, even if it depends on many frequencies. We extensively exploit this fact in the present work.

In this paper we arrange the methodology of [30] to deal with quasi-periodic signals depending on more than one frequency. A rough approximation[1] of the frequency to be computed is used to construct a new quasi-periodic signal having the same frequencies. The goal is that the iterates of the unfolded signal rotate around the origin and that the dynamics of the argument is leaded by this particular frequency. Now, the object projected onto the circle is not a curve, but a strip (that can be viewed as a planar projection of a torus whose dimension is the number of basic frequencies of the signal). Under suitable conditions, the unfolded signal induces a quasi-periodically forced circle diffeomorphism. There is no general result ensuring that the dynamics of a given quasi-periodically forced circle map is conjugate to a rigid rotation (if this holds, conjugation depends quasi-periodically on the forcing frequencies). Existence of the conjugation is not guaranteed by any nonresonance condition nor by the smoothness of the map (we refer to [16, 17]). In the present context, if the projection truly defines such a map, then it is conjugate to a rotation by construction. This is because the projected signal is already quasi-periodic. As noted before, we do not require this forced circle map to be well-defined. In practice, we only need a projected signal where the target frequency leads the rotation, so we can apply the averaging-extrapolation methodology to refine it.

Let us summarize some features of the method. The computation of frequencies is carried out without computing simultaneously a Fourier representation of the signal. Fourier coefficients can be obtained a posteriori, by slightly modifying the procedure for calculating the

[1]Sometimes this approximation is given by the context or by a preliminary study of the signal using a DFT-based method.

frequencies. Computation of frequencies is performed individually, so we can focus on one in particular. The same holds for the corresponding Fourier coefficient. The presented methodology is specially well-suited if we are are able to compute a large number of iterates of the signal with high precision. Then, in most of the cases the method is capable of computing frequencies with great accuracy at a reasonable computational cost. As a conclusion, once we have an approximation to a particular frequency, the presented averaging-extrapolation approach can be viewed as a refinement process for it. Although this is not the ultimate purpose of this work, the proposed methodology can be arranged to get the required approximations.

From a theoretical viewpoint, the accuracy of the method is not constrained by the number of significant Fourier harmonics required to approximate the quasi-periodic signal nor by the number of basic frequencies of the problem. It is also worth mentioning that, after the signal has been successfully unfolded, the cost to calculate any new iterate is not conditioned by the accuracy that we want to achieve for the refined frequency. Meanwhile, the accuracy expected using the collocation procedure of [13, 14] is limited by the truncation of the Fourier series. Indeed, if the problem has many basic frequencies or the Fourier coefficients do not decrease fast enough, then performing high accuracy computation by fitting the Fourier expansion requires to solve a system of large dimension. In the framework of the presented averaging-extrapolation construction, more precision can be obtained by computing more iterates of the signal (or, in the best case scenario, by simply increasing the extrapolation order). This is done without increment of the memory cost and with a computational cost which is essentially the cost of computing the iterates of the signal. In fact, if the signal is obtained by numerical integration of a vector field, the bottleneck in the computation time is the evaluation of the iterates and the cost of the method is almost negligible.

The paper is divided into two main parts. In section 2 we present the methodology for performing frequency analysis and related computations. This includes an informal exposition of the key ideas behind the "unfolding process" and also a complete description of the algorithms. We pay special attention to some subtle details so that the interested reader can implement this methodology obtaining an efficient performance. In section 3 we illustrate the presented methodology with the study of the vicinity of a Lagrangian equilibrium point of the Restricted Three Body Problem Sun-Jupiter-asteroid. We compute the frequencies for different sets of initial conditions to enhance some of the features of the methodology. We consider also a multicircular model where the effect of additional planets is taken into account.

2 Description of the averaging-extrapolation methods

In this section we present an averaging-extrapolation procedure for the computation of frequencies and amplitudes of a quasi-periodic signal. After introducing the problem in section 2.1, we summarize the main ideas behind our approach in section 2.2. We present our unfolding approach to single out a particular frequency in section 2.3. In section 2.4, we explain the averaging-extrapolation methodology to compute ("refine") this frequency. In section 2.5 we arrange the averaging-extrapolation construction to the computation of the Fourier coefficients of the signal, while in section 2.6 we discuss how we can get approximations to the frequencies in the framework of the presented approach. In section 2.7 we test the presented methods by considering an example with known frequencies.

2.1 Setting of the problem

In this section we set some basic notations and properties of quasi-periodic signals.

Definition 2.1. *Let $\mathbb{T}^r = \mathbb{R}^r/(2\pi\mathbb{Z})^r$ be the r-dimensional standard torus. We say that a complex sequence $\{z_n\}_{n\in\mathbb{Z}}$ is a quasi-periodic signal with frequency vector $\omega \in \mathbb{R}^r$, if there exists $\gamma : \mathbb{T}^r \to \mathbb{C}$ such that $z_n = \gamma(n\omega)$, $\forall n \in \mathbb{Z}$. If we denote the Fourier expansion of γ as*

$$\gamma(\theta) = \sum_{k\in\mathbb{Z}^r} \hat{\gamma}_k \mathrm{e}^{\mathrm{i}\langle k,\theta\rangle}, \qquad \hat{\gamma}_k = \frac{1}{(2\pi)^r}\int_{\mathbb{T}^r} \gamma(\theta)\mathrm{e}^{-\mathrm{i}\langle k,\theta\rangle} d\theta,$$

then we have the relation

$$z_n = \gamma(n\omega) = \sum_{k\in\mathbb{Z}^r} \hat{\gamma}_k \mathrm{e}^{\mathrm{i}n\langle k,\omega\rangle}. \tag{1}$$

Remark 2.2. *Considering complex-valued signals simplifies the exposition of the method. The presented approach also works if $\{x_n\}$ is a real-valued quasi-periodic signal. The method itself will turn it into a complex-valued one. If we have a vector-valued signal, $x_n = (x_n^1, \dots, x_n^l)$, then we have the chance of dealing with one of the components or to built a complex signal from them (for example, $z_n = x_n^1$, $z_n = x_n^1 + \mathrm{i}x_{n+1}^1$ or $z_n = x_n^1 + \mathrm{i}x_n^2$). As a general rule, it will be very useful if we can define z_n so that it "turns" around the origin (or around any other point) with a rotation frequency that is close to the one that we wish to calculate. This can save many computations.*

Remark 2.3. *If ω verifies nonresonance conditions $\langle k,\omega\rangle + 2\pi m \neq 0$, for any $k \in \mathbb{Z}^r \setminus \{0\}$ and $m \in \mathbb{Z}$, then ω is called a vector of basic frequencies of the signal. If these nonresonance conditions are not meet, then we can rewrite $\{z_n\}$ in terms of a new frequency vector, with a less number of frequencies. Besides nonresonance, we are going to assume that ω verifies Diophantine conditions of the form*

$$|\mathrm{e}^{\mathrm{i}\langle k,\omega\rangle} - 1| \geq \frac{C}{|k|_1^\tau}, \qquad \forall k \in \mathbb{Z}^r \setminus \{0\}, \tag{2}$$

for some $C, \tau > 0$, where $|k|_1 := |k_1| + \cdots + |k_r|$. It is well-known that if $\tau > r$, then the subset of $\omega \in \mathbb{R}^r$ for which conditions (2) *do not hold, for any $C > 0$, has zero Lebesgue measure (see [6]).*

Remark 2.4. *The vector of basic frequencies $\omega \in \mathbb{R}^r$ is not univocally defined. If we perform the transformation $\omega \mapsto M\omega + 2\pi k$, with $k \in \mathbb{Z}^r$ and M an unimodular matrix —i. e., $M \in \mathbb{M}_{r\times r}(\mathbb{Z})$ with $\det(M) = \pm 1$, then we obtain an equivalent vector of basic frequencies. We have to be aware of this fact when performing the frequency analysis. On the one hand, such property must be taken into account to correctly determine a set of basic frequencies. On the other hand, if the Fourier coefficient $\hat{\gamma}_{e_j}$ is small, then computing directly ω_j can be difficult. We have the chance of addressing its computation by dealing with another integer combination of basic frequencies $\langle k, \omega\rangle$, with $k_j \neq 0$, having a largest Fourier coefficient $\hat{\gamma}_k$.*

Remark 2.5. *We restrict the exposition to analytic quasi-periodic signals, although large enough differentiability suffices. The differentiability required depends on the exponent τ of the Diophantine condition* (2) *and on the selected extrapolation orders (we refer to [36] for more details). Analyticity of $\{z_n\}$ means that γ in* (1) *is an analytic function. Specifically, there exists positive constants ρ and M such that $|\hat{\gamma}_k| \leq M\mathrm{e}^{-\rho|k|_1}$.*

Remark 2.6. *Quasi-periodic signals like* (1) *are typically associated to a discrete dynamical system. This system can be defined by a map $F : U \subset \mathbb{R}^l \to \mathbb{R}^l$ or, more in general, by a quasi-periodically forced map $G : U \times \mathbb{T}^s \to \mathbb{R}^l \times \mathbb{T}^s$, of the form $G(x, \hat{\theta}) = (g(x, \hat{\theta}), \hat{\theta} + \hat{\omega})$, where $U \subset \mathbb{R}^l$ and $\hat{\omega} \in \mathbb{R}^s$. Let us suppose that $\gamma : \mathbb{T}^r \to \mathbb{R}^l$ is a parameterization of a quasi-periodic invariant torus of any of these maps. In the "autonomous case" we have $F(\gamma(\theta)) = \gamma(\theta + \omega)$. For quasi-periodically forced maps, the invariance condition is $g(\gamma(\theta), \hat{\theta}) = \gamma(\theta + \omega)$, where $\theta = (\widetilde{\theta}, \hat{\theta})$ and $\omega = (\widetilde{\omega}, \hat{\omega})$ (i. e., the torus "captures" the frequencies of the forcing). If we take an initial condition on the torus, $x_0 = \gamma(\theta_0)$, for some $\theta_0 \in \mathbb{T}^r$, then $x_n = F^n(x_0)$ or $(x_n, n\hat{\omega}) = G^n(x_0, \hat{\theta}_0)$ define a vector-valued quasi-periodic signal given by $x_n = \gamma(\omega n + \theta_0)$.*

Remark 2.7. *Let us consider a quasi-periodic function of continuous variable $f : \mathbb{R} \to \mathbb{C}$, i. e., $f(t) = F(\widetilde{\omega}t)$, with $F : \mathbb{T}^r \to \mathbb{C}$ and $\widetilde{\omega} \in \mathbb{R}^r$. We can introduce a (discrete-time) quasi-periodic signal as $z_n = f(nT)$, for a fixed $T > 0$. Then, $\{z_n\}$ has frequency vector $\omega = T\widetilde{\omega}$. In this situation we have to be aware of some facts due to the time discretization.*

(a) *Nonresonance conditions for a vector of basic frequencies of a continuous-time quasi-periodic signal are $\langle k, \widetilde{\omega}\rangle \neq 0$, $\forall k \in \mathbb{Z}^r \setminus \{0\}$. To ensure that $T\widetilde{\omega}$ is a nonresonant frequency vector for the discretized signal, we need that $T \neq \frac{2\pi m}{\langle k, \widetilde{\omega}\rangle}$, for any $k \in \mathbb{Z}^r \setminus \{0\}$ and $m \in \mathbb{Z}$. It is equivalent to say that the $(r + 1)$-dimensional vector $(\widetilde{\omega}, 2\pi/T)$ is a nonresonant frequency vector of a continuous-time quasi-periodic signal —i. e., we are adding an "artificial" frequency when performing the time-discretization. In fact, an "exact resonance" between T and $\widetilde{\omega}$ is not a bad thing, because then we are not adding a new frequency due to the discretization (see Remark 2.8 for comments on time-dependent differential equations). Numerically, problems arise when we are close to a low-order resonance, i. e., $T \approx \frac{2\pi m}{\langle k, \widetilde{\omega}\rangle}$, with k and m not "too big". Then, we are going to have bad Diophantine conditions for ω (a small C in* (2)*). This is the worst situation for our methods. However, in the framework of this paper, the computation of $\widetilde{\omega}$ will follow from* *the prior knowledge of an approximate value $\widetilde{\omega}^0 \approx \widetilde{\omega}$. Then, we have the chance to ensure, numerically, that there are no low-order resonances between $\widetilde{\omega}^0$ and T.*

(b) *If $\omega \in \mathbb{R}^r$ is a vector of basic frequencies of the discretized signal, then we cannot always claim that ω/T is a vector of basic frequencies of the continuous-time signal. It turns out that we can select $\widetilde{\omega} = \omega/T + 2\pi m/T$, for some $m \in \mathbb{Z}^r$. Let $\widetilde{\omega}_0$ be an initial approximation to one of the components of $\widetilde{\omega}$, say $\widetilde{\omega}_0 \approx \widetilde{\omega}_1 > 0$. Then, it is natural to select $T\widetilde{\omega}_0$ as initial approximation for a frequency of the discretized signal. If after application of our methodology we end computing a refined value ω_1 such that $\omega_1 \approx T\widetilde{\omega}_1^0$, then it is quite natural that ω_1/T is a refined value for $\widetilde{\omega}_1$. However, we have to be careful with the "size" of the selected T. This is because our methodology is based on tracking how the argument of the discretized signal turns around the origin. Then, we must select T so that $T\widetilde{\omega}_1 < 2\pi$. Otherwise, what we compute is the value of $T\widetilde{\omega}_1$ minus the turns. See Remark 3.3 for additional comments.*

Remark 2.8. *A particular case of Remark 2.7 is the study of a quasi-periodic invariant torus of an ordinary differential equation. Any trajectory on the torus defines a quasi-periodic function of continuous variable. Then, the discretization described in Remark 2.7 can be dealt as follows:*

(a) *If the equation is periodic or quasi-periodic in time, it is natural to perform stroboscopic sections. Indeed, in the periodic case one can select T as the period of the system. In the quasi-periodic one, if $\omega_1 > 0$ is a basic frequency of the differential equation, then it is natural to select $T = 2\pi/\omega_1$ (i. e., we are performing a Poincaré section by the angle associated to this frequency). This approach can also be used in the autonomous case in order to remove a frequency already known (for instance, a "dominant frequency", so that we "magnify" the contribution of the Fourier coefficients of the other ones). To do that, it is important to know it very accurately. Otherwise, instead of removing a frequency we are replacing it by a close to resonant one (specifically, if ω_0 is this frequency and we take $T = 2\pi/\omega_1$, then we are adding the frequency $2\pi\omega_0/\omega_1$), which can lead numerics to fail.*

(b) *In the autonomous case, one can define the discretized signal through a Poincaré section by a transversal hypersurface of the phase space. This has the advantage of removing a frequency of the quasi-periodic continuous-time signal instead of adding a new one.*

2.2 Informal scheme of the main construction

In this section we outline the basic aspects of our approach to the computation of frequencies. We focus on the schematic exposition of the unfolding process, omitting details on the computation (refinement) of the frequencies and explanations on the methods to accelerate the converge of the procedure. Let us consider a "toy example" given by the signal

$$z_n = A\mathrm{e}^{\mathrm{i}n\omega_1} + B\mathrm{e}^{\mathrm{i}n(\omega_1+\omega_2)}, \tag{3}$$

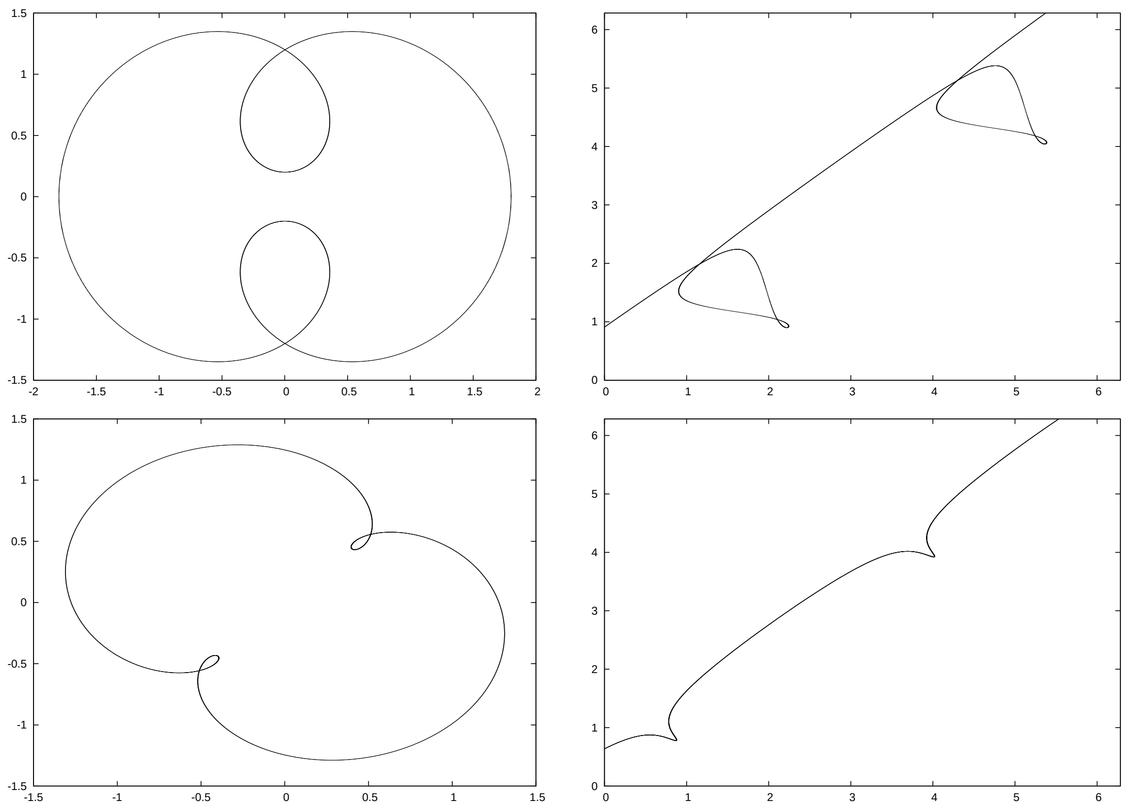

Figure 1: The signal (3) for $A = 1$, $B = 0.8$, $\omega_1 = (\sqrt{5}-1)\pi/8 \approx 0.4854$ and $\omega_2 = 2\omega_1$. Top plots show the planar curve described by (3) and the correspondence $\mathbb{R} \to \mathbb{R}$ generated by a lift of the complex argument of the iterates. Bottom plots correspond to the unfolded signal (6) and its lift, with $\omega_0 = \omega_1 + 0.1$ and $L = 4$. As a matter of fact, the signal is completely unfolded for $L = 5$ and the lift becomes a graph.

for some $A, B \in \mathbb{C}$, with $\omega_j > 0$ and $\omega_j/2\pi \notin \mathbb{Q}$, for $j = 1, 2$. Note that if $\omega_1/\omega_2 \in \mathbb{Q}$, then (3) densely fills a planar curve (i. e., there is only one independent frequency). For general values of A and B this curve is non-injective and can have many folds (see Figure 1). If $\omega_1/\omega_2 \notin \mathbb{Q}$, then the signal can be viewed as a planar projection of a 2-dimensional torus in $\mathbb{R}^3$. Throughout the exposition we concentrate on the computation of ω_1.

The simplest situation is when $B = 0$ and $A \neq 0$. Note that z_n belongs to the complex circle of radius $|A|$ centered at the origin. By means of the argument we can project this signal onto $\mathbb{T} = \mathbb{R}/2\pi\mathbb{Z}$. Then, the correspondence $z_n \mapsto z_{n+1}$ generates the rigid rotation $x \in \mathbb{T} \mapsto x + \omega_1 \in \mathbb{T}$, with rotation number $\omega_1/2\pi$. The fundamental point of our approach is that if $A \cdot B \neq 0$, but $|B/A|$ is small enough, then the projection of the signal onto the unit circle also generates an orbit with "rotation number" $\omega_1/2\pi$. Next we assume that $0 < |B/A| < 1$. In this case, we can find a simple expression for the dynamics of the argument. In fact, there exists a

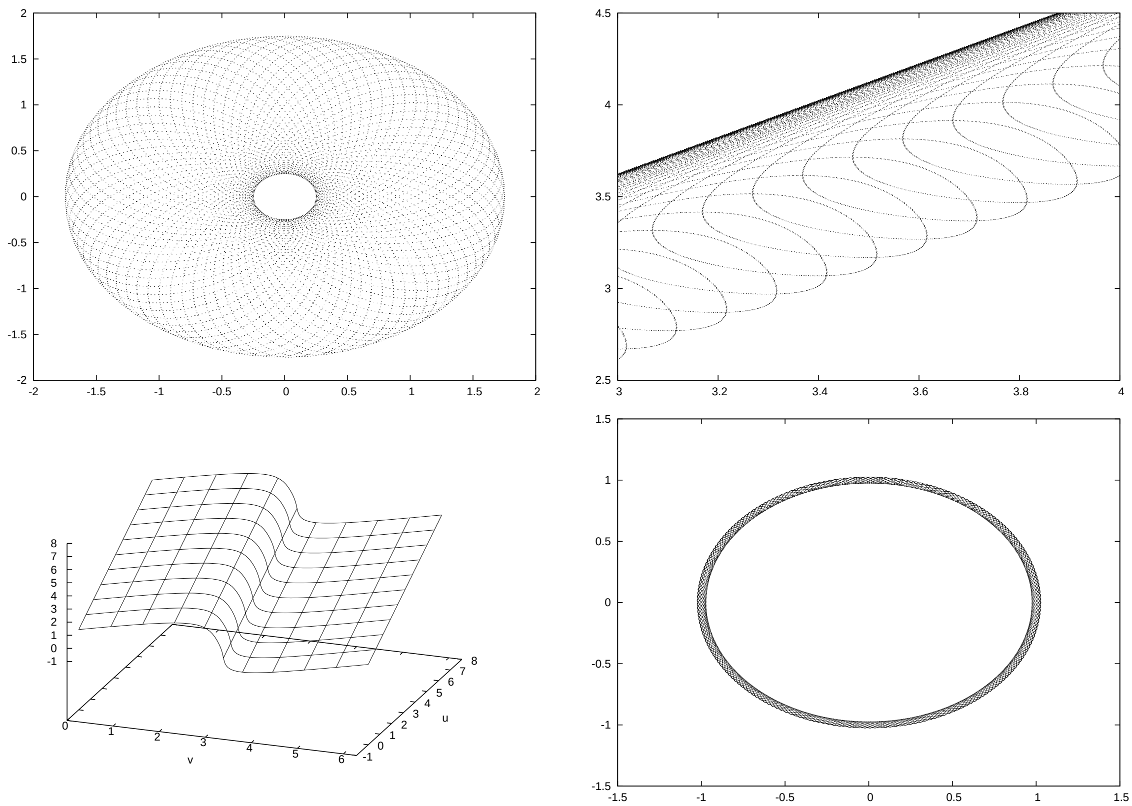

Figure 2: The signal (3) for $A = 1$, $B = 0.75$, $\omega_1 = (\sqrt{5} - 1)\pi/8$ and $\omega_2 = (\sqrt{2} - 1)\pi/4 \approx 0.3253$. Top-left plot shows how the dynamics densely fills the annulus that contains the orbit. Top-right plot shows the correspondence $\mathbb{R} \to \mathbb{R}$ generated by a lift of the signal. This correspondence fills a strip in $\mathbb{R}^2$ (the plot shows how the dynamics organizes this strip). Bottom-left plot shows the same lift, but now computed as $\mathbb{R} \times \mathbb{T} \to \mathbb{R}$. Synthetically, this lift is generated by the transformation $(u, v) = (\arg(z_n), n\omega_2) \mapsto \arg(z_{n+1})$ (i. e., v is the angle associated to ω_2, which is interpreted as a quasi-periodic forcing). The result looks as a smooth (but folded) surface. Finally, bottom-right plot shows the unfolded signal (6) for $\omega_0 = \omega_1$ (the exact frequency) and $L = 20$. The dynamics becomes a perturbation of a rotation of angle ω_1 on the unit circle.

periodic and analytic function $\varphi(\theta) = \arg(1 + (B/A)e^{i\theta})$ such that[2]

$$z_n = |A + Be^{in\omega_2}|e^{i(n\omega_1 + \arg(A) + \varphi(n\omega_2))}, \tag{4}$$

so the iterates $x_n = \arg(z_n)$ are given by

$$x_n = n\omega_1 + \arg(A) + \varphi(n\omega_2). \tag{5}$$

Now we consider two different situations:

[2]If $|B/A| > 1$, then the analytic continuation of $\varphi(\theta)$ is not periodic, but $\varphi(\theta + 2\pi) = \varphi(\theta) + 2\pi$.

- *We have a single independent frequency.* Specifically, we assume that $\omega_2 = m\omega_1$, for some $m \in \mathbb{Z}$. If $|B/A|$ is small enough such that $|m\varphi'(\theta)| < 1$, $\forall \theta \in \mathbb{T}$, then the correspondence $x_n \mapsto x_{n+1}$ generates a circle diffeomorphism $f : \mathbb{T} \to \mathbb{T}$. By construction, f is conjugate to the rigid rotation $x \mapsto x + \omega_1$. The conjugation is $\theta \mapsto \theta + \varphi(m\theta)$. In this case, we speak about a "projectable" curve or signal, in the sense that the mere "projection" of the iterates onto $\mathbb{T}$ generates a circle diffeomorphism with the same frequency as the signal. To compute ω_1, the relevant fact is that we can evaluate a lift of f to $\mathbb{R}$ just by tracking how the iterates of the signal rotate around the origin (adding the accumulated turns to the argument of z_n). Indeed, formula (5) gives the expression of the iterates by the lift. As shown in Section 2.4, the averaging-extrapolation methodology of [36] allows computing ω_1 from the iterates of the lifted signal. To this end, we will see that it is not necessary that $\{x_n\}$ generates a circle diffeomorphism, so the condition $|m\varphi'(\theta)| < 1$ is too strong in practice.

- *We have two rationally independent frequencies.* Since $|B/A| < 1$, the correspondence $x_n \mapsto x_{n+1}$ does not generate a circle map, but a quasi-periodically forced circle map with ω_2 as the frequency of the forcing. This map takes the form of a skew-product, $(\theta_1, \theta_2) \in \mathbb{T} \times \mathbb{T} \mapsto (f(\theta_1, \theta_2), \theta_2 + \omega_2) \in \mathbb{T} \times \mathbb{T}$. The transformation f is conjugate to the rigid rotation $x \mapsto x + \omega_1$ by a conjugation that depends quasi-periodically on θ_2, with frequency ω_2. This conjugation is $(\theta_1, \theta_2) \mapsto (\theta_1 + \varphi(\theta_2), \theta_2)$. If we compute the lift to $\mathbb{R}$ of the argument of the iterates $\{z_n\}$, it is also given by (5). Although now the right-hand side of (5) depends quasi-periodically on ω_2, it turns out that ω_1 can still be computed by averaging-extrapolation methods.

If $|B/A| \geq 1$, discussions above are no longer true. Nevertheless, given an approximation of the frequency that we want to compute, $\omega_0 \simeq \omega_1$, we can built a new quasi-periodic signal from (3), having the same frequencies, with a slightly modified A but with a smaller B. In fact, given $L \in \mathbb{N}$, we introduce

$$z_n^{(L,\omega_0)} = \frac{1}{L} \sum_{m=n}^{L+n-1} z_m \mathrm{e}^{\mathrm{i}(n-m)\omega_0} = \frac{A}{L} \frac{1 - \mathrm{e}^{\mathrm{i}(\omega_1 - \omega_0)L}}{1 - \mathrm{e}^{\mathrm{i}(\omega_1 - \omega_0)}} \mathrm{e}^{\mathrm{i}n\omega_1} + \frac{B}{L} \frac{1 - \mathrm{e}^{\mathrm{i}(\omega_1 + \omega_2 - \omega_0)L}}{1 - \mathrm{e}^{\mathrm{i}(\omega_1 + \omega_2 - \omega_0)}} \mathrm{e}^{\mathrm{i}n(\omega_1 + \omega_2)}. \tag{6}$$

Note that $z_n^{(L,\omega_0)}$ involves the sum of the L consecutive phase-shifted iterates $z_m \mathrm{e}^{-\mathrm{i}m\omega_0}$, $m = n, \ldots, L + n - 1$. To understand the reason of Definition (6), we note that in the "limit case" $\omega_0 = \omega_1$ we get

$$z_n^{(L,\omega_1)} = A\mathrm{e}^{\mathrm{i}n\omega_1} + \frac{B}{L} \frac{1 - \mathrm{e}^{\mathrm{i}\omega_2 L}}{1 - \mathrm{e}^{\mathrm{i}\omega_2}} \mathrm{e}^{\mathrm{i}n(\omega_1 + \omega_2)}. \tag{7}$$

Thus, for large enough values of L, the signal $z_n^{(L,\omega_1)}$ turns out to be "projectable" onto $\mathbb{T}$, given rise to a circle map or to a quasi-periodically forced circle map —depending on the case— with rotation frequency ω_1. If $\omega_0 \approx \omega_1$ are close enough, then the behaviour of $z_n^{(L,\omega_0)}$ is similar for "moderately large" values of L (see Remark 2.12). In Section 2.3 we show that if we have a generic quasi-periodic signal, with an arbitrary number of frequencies, then the same construction is useful in order to single out a particular frequency ω_1. This construction is illustrated in Figure 1 (ω_1 and ω_2 are dependent) and Figure 2 (ω_1 and ω_2 are independent). Due to the observed geometrical effect, we refer to this procedure as unfolding of the signal.

We observe that if the signal is very folded (for example, if $|B/A|$ is very large in (3)), then it can be expensive to generate a projectable signal (even impossible if $|\omega_1 - \omega_0|$ is not extremely small). From the computational viewpoint, "expensive" means that we are forced to take large values of L in (6) in order to decrease the contribution of the Fourier coefficients different from the one of $\mathrm{e}^{in\omega_1}$. Fortunately, in applications it is not necessary to completely unfold the signal. Next, we try to clarify this assertion.

Let us concentrate on a generic analytic and quasi-periodic signal $\{z_n\}$ with one frequency $\omega_1 \in (0, 2\pi)$. Although the corresponding curve is non-projectable, we can consider the dynamics of the argument along the iterates. Indeed, if $x_n = \arg(z_n)$, then the couples (x_n, x_{n+1}) generate a correspondence on the circle given by $x_n \in \mathbb{T} \mapsto x_{n+1} \in \mathbb{T}$. If we lift this correspondence to $\mathbb{R}$ along the whole curve, then we obtain a correspondence $\mathbb{R} \mapsto \mathbb{R}$. The lift describes how the argument of the iterates evolves along the origin, regardless of whether it moves forwards or backwards as a function of n (lift must rise 2π for every turn of the signal). Although in general this lift is not a graph, it is natural to expect that it is given by an analytic curve. This is illustrated in Figure 1 for the signal in (3). By following the evolution of the lift along the iterates, we can define the rotation frequency $\bar{\omega}_1$ of the signal in a complete analogy to the rotation number of a circle map. Specifically, $\bar{\omega}_1/2\pi$ gives the average number of turns by iterate. The important thing is that not only the mere definition $\bar{\omega}_1 = \lim_{n\to\infty}(x_n - x_0)/n$ is valid in this case, but the averaging-extrapolation procedure of [36] works as well for accelerating the convergence to $\bar{\omega}_1$.

We note that $\bar{\omega}_1$ is not necessarily related to any frequency of the signal. If we have a good enough approximation of ω_1, then we can unfold $\{z_n\}$ by means of (6) until we get a projectable signal $\{z_n^{(L,\omega_0)}\}$ giving rise to a circle map of frequency ω_1. Hence, we truly have $\bar{\omega}_1 = \omega_1$ for the unfolded signal. Moreover, practice shows that removing the main folds suffices to set the target frequency as a rotation frequency of this "partially unfolded signal", provided that the folds of the new signal are small compared with ω_1. These small folds are averaged out when computing the rotation frequency. Performing partial unfolding is computationally less demanding.

Let us summarize the discussion above for the signal (3) when $\omega_1/\omega_2 \in \mathbb{Q}$. The correspondence of $\mathbb{R}$ induced by the lift is analytic except when $|A| = |B|$. If $\omega_2 = m\omega_1$, then the condition $|m\varphi'| < 1$ in (5) ensures that the signal is projectable. In general, to ensure that ω_1 is the frequency that leads the rotation we need the weaker condition $|B/A| < 1$. This is enough for our purposes. When $|B/A| > 1$ the rotation frequency is $\omega_1 + \omega_2$. The unfolding method defines a new signal having the same frequencies but with a smaller value of B.

For a quasi-periodic signal $\{z_n\}$ with many basic frequencies, $\omega \in \mathbb{R}^r$, the picture is very similar. Let ω_0 be a numerical approximation to one of the frequencies, say $\omega_0 \approx \omega_1$. Assume that using (6) we can (partially) unfold the signal such that ω_1 becomes the leading frequency of the rotation around the origin of $\{z_n^{(L,\omega_0)}\}$. Then, the lift to $\mathbb{R}$ of the dynamics of the argument of $\{z_n^{(L,\omega_0)}\}$ generates a quasi-periodically forced correspondence of $\mathbb{R}$, where the frequencies of the forcing are the $r-1$ remaining components of ω. We expect this lift to be given by an analytic expression in $\theta \in \mathbb{T}^r$, where θ are the angle variables of the torus that parameterizes the quasi-periodic signal (see Definition 2.1). Then, the methodology of [36] is well-suited for computing ω_1 from the iterates of this lift.

Remark 2.9. *To plot the lifts of these signals (Figures 1 and 2) we display the couples* (x_n, x_{n+1})*, where* $x_n = \arg(z_n)$*. We must take suitable determinations of the arguments (defined modulus* 2π*) in order to achieve the usual translation properties of the lift. As we have an explicit expression for the quasi-periodic signal* (3)*, we can define* $Z(\theta_1, \theta_2) = A\mathrm{e}^{\mathrm{i}\theta_1} + B\mathrm{e}^{\mathrm{i}(\theta_1+\theta_2)}$ *so that* $z_n = Z(n\omega_1, n\omega_2)$*. This allows using a continuous variable* $t \in \mathbb{R}$ *instead of the discrete one* n*, so that the plots can be made in terms of* $z(t) = Z(\omega_1 t, \omega_2 t)$*. Then, the lift can be parameterized as* $t \mapsto (x(t), x(t+1))$*, where* $x(t) = \arg(z(t))$*. This corresponds to take the closure of the lift computed only for the discrete iterates* z_n*.*

2.3 Unfolding of the signal to isolate a frequency

In this section we describe in detail the unfolding process of a quasi-periodic signal that we have already outlined in Section 2.2. The goal is to build a new signal having the target frequency as a rotation frequency around the origin. This allows computing this particular frequency, with high accuracy, by the methodology of Section 2.4. As we discussed in the introduction, the presented construction is an adaptation of the approach of [30].

This section is organized as follows. In Section 2.3.1 we present the basic features of the unfolding process. This introduces a new quasi-periodic signal by a weighted average, inspired in the DFT, of some consecutive iterates. Under appropriate conditions, the convergence rate is of $\mathcal{O}(1/L)$, where L is the number of iterates involved in the average. In Sections 2.3.2 and 2.3.3 we present higher order averages that accelerate the convergence of the unfolding process up to orders $\mathcal{O}(1/L^2)$ and $\mathcal{O}(1/L^p)$, respectively.

2.3.1 First order unfolding

Here we present the fundamental method to unfold a quasi-periodic signal, generalizing the motivating ideas discussed in Section 2.2. The cornerstone is the following construction.

Definition 2.10. *Let* $\{z_n\}_{n\in\mathbb{Z}}$ *be a complex-valued quasi-periodic signal as in Definition 2.1. We assume that* $\{z_n\}$ *is analytic (see Remark 2.5) and that the frequency vector* $\omega \in \mathbb{R}^r$ *verifies Diophantine conditions* (2)*. For any* $\omega_0 \in \mathbb{R}$ *and* $L \in \mathbb{N}$*, we define the following iterates:*

$$z_n^{(L,\omega_0)} = \frac{1}{L} \sum_{m=n}^{L+n-1} z_m \mathrm{e}^{\mathrm{i}(n-m)\omega_0}. \tag{8}$$

It is easy to see that for most[3] of ω_0, the sequence $\{z_n^{(L,\omega_0)}\}_{n\in\mathbb{Z}}$ is a quasi-periodic signal with the same frequency vector ω. Indeed,

$$z_n^{(L,\omega_0)} = \gamma^{(L,\omega_0)}(n\omega) = \sum_{k\in\mathbb{Z}^r} \hat{\gamma}_k^{(L,\omega_0)} \mathrm{e}^{\mathrm{i}n\langle k,\omega\rangle}, \tag{9}$$

where the new Fourier coefficients are

$$\hat{\gamma}_k^{(L,\omega_0)} = \frac{\hat{\gamma}_k}{L} \sum_{m=n}^{L+n-1} \mathrm{e}^{\mathrm{i}(m-n)(\langle k,\omega\rangle-\omega_0)} = \frac{\hat{\gamma}_k}{L} \frac{1-\mathrm{e}^{\mathrm{i}L(\langle k,\omega\rangle-\omega_0)}}{1-\mathrm{e}^{\mathrm{i}(\langle k,\omega\rangle-\omega_0)}}. \tag{10}$$

Assume that ω_0 is one of the frequencies of the signal, say $\omega_0 = \omega_1$. Omitting the dependence on ω_0 we write $z_n^{(L)} = z_n^{(L,\omega_1)}$. Then, expression (10) takes the form (compare with (7))

$$z_n^{(L)} = \sum_{k\in\mathbb{Z}^r} \hat{\gamma}_k^{(L)} \mathrm{e}^{\mathrm{i}n\langle k,\omega\rangle}, \quad \hat{\gamma}_{e_1}^{(L)} = \hat{\gamma}_{e_1}, \quad \hat{\gamma}_k^{(L)} = \frac{\hat{\gamma}_k}{L} \frac{1-\mathrm{e}^{\mathrm{i}L(\langle k,\omega\rangle-\omega_1)}}{1-\mathrm{e}^{\mathrm{i}(\langle k,\omega\rangle-\omega_1)}}, \ \text{ for } k \neq e_1.$$

Since the signal is analytic and ω Diophantine, then $\hat{\gamma}_k^{(L)} = \mathcal{O}(\mathrm{e}^{-\rho|k|_1}|k-e_1|_1^{\tau}/L)$, if $k \neq e_1$. Consequently, for large enough values of L, the "unfolded signal" $\{z_n^{(L)}\}$ becomes a quasi-periodic perturbation of a planar rotation of angle ω_1. Indeed, provided that $\hat{\gamma}_{e_1} \neq 0$,

$$z_n^{(L)} = \hat{\gamma}_{e_1} \mathrm{e}^{\mathrm{i}n\omega_1}(1+\Gamma^{(L)}(n\omega)), \tag{11}$$

where $\Gamma^{(L)} : \mathbb{T}^r \to \mathbb{C}$ is analytic and $\Gamma^{(L)} = \mathcal{O}(1/L)$. We consider the projection of this orbit onto the circle $\mathbb{T} = \mathbb{R}/2\pi\mathbb{Z}$ through the argument,

$$\begin{array}{ccl} \mathbb{C} & \longrightarrow & \mathbb{T} \\ z_n^{(L)} & \longmapsto & x_n^{(L)} = \arg(z_n^{(L)}). \end{array} \tag{12}$$

If $\Gamma^{(L)}$ is small enough, then this projection introduces a quasi-periodic signal $\{x_n^{(L)}\}$ on $\mathbb{T}$, where the frequency ω_1 leads the rotation. Specifically, by using polar coordinates we can write

$$z_n^{(L)} = |\hat{\gamma}_{e_1}| \cdot |1+\Gamma^{(L)}(n\omega)| \mathrm{e}^{\mathrm{i}(n\omega_1+\phi^{(L)}(n\omega))},$$

where $\phi^{(L)} : \mathbb{T}^r \to \mathbb{R}$ is an analytic function, with $\phi^{(L)} = \mathcal{O}(1/L)$. Then, $\{x_n^{(L)}\}$ is defined by taking modulo 2π on the expression

$$x_n^{(L)} = n\omega_1 + \phi^{(L)}(n\omega). \tag{13}$$

The key is that the lift to $\mathbb{R}$ of $\arg(z_n^{(L)})$ is precisely given by formula (13). This is the cornerstone of the averaging-extrapolation method of section 2.4 for computing ω_1.

[3]The set of values of ω_0 for which $z_n^{(L,\omega_0)}$ is not quasi-periodic has zero Lebesgue measure. This theoretical situation plays no role in this work.

Remark 2.11. *Let us suppose that $\phi^{(L)}$ is small enough such that $\Psi(\theta) = (\theta_1 + \phi^{(L)}(\theta), \hat{\theta})$ is a change of variables of $\mathbb{T}^r$, where $\theta = (\theta_1, \hat{\theta})$. Then, the correspondence $x_n^{(L)} \mapsto x_{n+1}^{(L)}$ induces a quasi-periodically forced circle map, where the frequencies of the forcing are $\hat{\omega} = (\omega_2, \ldots, \omega_r)$. This map takes the form $F(\theta) = (f(\theta), \hat{\theta} + \hat{\omega})$, where f is defined through the relation*

$$f(\theta_1 + \phi^{(L)}(\theta)) = \theta_1 + \omega_1 + \phi^{(L)}(\theta + \omega).$$

Then, $x_{n+1}^{(L)} = f(x_n^{(L)}, n\hat{\omega})$. By construction, the dynamics of $x_n^{(L)}$ is conjugate to the rotation $x \mapsto x + \omega_1$, by a conjugation that depends quasi-periodically on $\hat{\theta}$. Specifically, $F \circ \Psi(\theta) = \Psi(\theta + \omega)$. If Ψ is not a change of variables, but expression (13) *holds, then the dynamics of $x_n^{(L)}$ is only semi-conjugate to a rotation. Although in this situation we do not have any kind of circle map, semi-conjugation suffices for our purposes (regardless of the size of $\phi^{(L)}$).*

A realistic setting is to suppose that we know an approximation ω_0 of ω_1, say $\omega_0 = \omega_1 + \varepsilon$. If ε is small enough, then it is natural to expect that we can choose $L = L(\varepsilon)$ such that the projection (12) of the "unfolded" signal $z_n^{(L,\omega_0)}$ has a similar behaviour as in the case $\omega_0 = \omega_1$. Specifically, we expect that we still have an expression like (13) for $x_n^{(L,\omega_0)}$, which is defined by the lift of $\arg(z_n^{(L,\omega_0)})$.

Remark 2.12. *If we want $z_n^{(L,\omega_0)}$ to behave as a perturbation of a rotation of angle ω_1, then it turns out that $L|\varepsilon|$ must be fairly small. This is required to ensure that $\hat{\gamma}_1^{(L,\omega_0)}$ in* (10) *remains close to $\hat{\gamma}_1$, while the other Fourier coefficients behave as $\mathcal{O}(1/L)$. Otherwise, perhaps it is impossible to set ω_1 as a leading frequency of the rotation (even for large values of L).*

Remark 2.13. *If $\varepsilon \neq 0$, then* (2) *does not provide lower bounds for the denominators of $\hat{\gamma}_k^{(L,\omega_0)}$ in* (10)*. The behaviour of these denominators vary depending on the particular value of $\omega_0 = \omega_1 + \varepsilon$ (resonances define a dense set). However, if ε is small, it will be very rare to find obstructions due to resonances. On the one hand, let $\mathcal{D}_{\varepsilon_0}$ be the set of values of ε, with $|\varepsilon| \leq \varepsilon_0$, for which we have*

$$|1 - \mathrm{e}^{\mathrm{i}(\langle k,\omega\rangle - \omega_0)}| \geq \frac{C/2}{|k - e_1|_1^\tau}, \qquad \forall k \in \mathbb{Z}^r \setminus \{e_1\}. \tag{14}$$

Then, the Lebesgue measure of $[-\varepsilon_0, \varepsilon_0] \setminus \mathcal{D}_{\varepsilon_0}$ admits an exponentially small bound on ε_0. On the other hand, if $\varepsilon \in [-\varepsilon_0, \varepsilon_0] \setminus \mathcal{D}_{\varepsilon_0}$, then we can guarantee (14) *up to a very large value of $|k|_1$ (precisely, up to $\mathcal{O}(1/\varepsilon_0^{1/\tau})$). As the Fourier coefficients $\hat{\gamma}_k$ are exponentially small on $|k|_1$, this means that the contribution of the remaining part of the Fourier series is small* per se*, with independence of any Diophantine bound. We do not formalize precisely this fact, but we refer to [21] where this idea is the keystone of the paper.*

Remark 2.14. *Among the drawbacks of the method, there are the obvious constrains of a signal having very low regularity*[4] *or having close-to-resonant frequencies (with a very small* C *in* (2) *and* (14)*). Another limitation is when the Fourier coefficient of the frequency we want to compute is small. For example, if the signal is generated by a dynamical system that contains a small quasi-periodic perturbation and we want to compute the frequencies of the perturbation. A similar scenario appears if the signal captures some small oscillations around a linearly stable quasi-periodic torus of a Hamiltonian system. In these cases, unfolding the signal to single out such frequency can be very difficult or even impossible. This does not imply that the method always fails to compute a frequency with small amplitude, but a very good approximation to this frequency is needed to unfold the signal and the cost of the unfolding can be quite expensive. Sometimes this constrain can be addressed by changing the target frequency (in the sense of Remark 2.4). As a general rule, to tackle this issue we can subtract to the original signal the Fourier polynomial associated to its "dominant frequencies" (assuming they have been already computed).*

Remark 2.15. *Even when the unfolding process is unsuccessful (perhaps* L *is not too large or the first approximation to* ω_1 *is too poor), in general the averaging-extrapolation methodology of section 2.4 applied to* $x_n^{(L,\omega_0)}$ *converges to a certain value* $\bar{\omega}_1$ *(usually with high accuracy). The issue is if* $\bar{\omega}_1$ *is a true frequency of the signal. Fortunately, if* $\bar{\omega}_1$ *is not a frequency then it is easy to realize about the mistake. This is discussed in Remark 2.35. Then, we must improve the unfolding process.*

In the best case scenario, the new signal $z_n^{(L,\omega_0)}$ tends to be a rotation with a convergence rate of $\mathcal{O}(1/L)$. This is the same speed that we have when computing the rotation number of a circle map by the definition. In general, this is not quite satisfactory in practice. The issue is that if a large L is required, then this increases the computational cost. At first glance, we can subtract the average of the signal as a simple (but useful) way to improve the unfolding process. In Sections 2.3.2 and 2.3.3 we describe a systematic procedure to accelerate the convergence of the unfolding.

2.3.2 Second order unfolding

To accelerate the unfolding we perform higher order averages and Richardson extrapolation. We start introducing the second order averages.

Definition 2.16. *Under the same notations and hypotheses of Definition 2.10, we introduce the sequences*

$$\mathcal{Z}_n^{(L,\omega_0,2)} = \sum_{l=1}^{L} \sum_{m=n}^{l+n-1} z_m \mathrm{e}^{-\mathrm{i}m\omega_0}, \qquad \widetilde{\mathcal{Z}}_n^{(L,\omega_0,2)} = \left(\frac{2}{L(L+1)} \mathcal{Z}_n^{(L,\omega_0,2)} \right) \mathrm{e}^{\mathrm{i}n\omega_0}. \tag{15}$$

[4] Finite differentiability means that $\hat{\gamma}_k$ is $\mathcal{O}(1/|k|_1^p)$. We require a sufficiently large p to justify our approach. We refer to [37] for an example where averaging-extrapolation methods have been adapted to address a problem with very low regularity.

Then, we define the following iterates:

$$z_n^{(2L,\omega_0,2)} = 2\widetilde{\mathcal{Z}}_n^{(2L,\omega_0,2)} - \widetilde{\mathcal{Z}}_n^{(L,\omega_0,2)}. \tag{16}$$

For most values of ω_0, the signal $\{z_n^{(2L,\omega_0,2)}\}_{n\in\mathbb{Z}}$ is quasi-periodic with frequency vector ω. As before, the limit case $\omega_0 = \omega_1$ is useful to illustrate the properties of the new iterates. Then, we write $\mathcal{Z}_n^{(L)} = \mathcal{Z}_n^{(L,\omega_1,2)}$ and compute

$$\begin{aligned}
\mathcal{Z}_n^{(L)} &= \sum_{l=1}^{L}\sum_{m=n}^{l+n-1}\sum_{k\in\mathbb{Z}^r}\hat{\gamma}_k \mathrm{e}^{\mathrm{i}(m-n)(\langle k,\omega\rangle-\omega_1)} \\
&= \frac{L(L+1)}{2}\hat{\gamma}_{e_1} + L\sum_{k\neq e_1}\hat{\gamma}_k\frac{\mathrm{e}^{\mathrm{i}n(\langle k,\omega\rangle-\omega_1)}}{1-\mathrm{e}^{\mathrm{i}(\langle k,\omega\rangle-\omega_1)}} - \sum_{k\neq e_1}\hat{\gamma}_k\frac{1-\mathrm{e}^{\mathrm{i}L(\langle k,\omega\rangle-\omega_1)}}{(1-\mathrm{e}^{\mathrm{i}(\langle k,\omega\rangle-\omega_1)})^2}\mathrm{e}^{\mathrm{i}(n+1)(\langle k,\omega\rangle-\omega_1)}.
\end{aligned}$$

Consequently,

$$\widetilde{\mathcal{Z}}_n^{(L)} = \hat{\gamma}_{e_1}\mathrm{e}^{\mathrm{i}n\omega_1} + \frac{2}{L+1}\mathcal{A}_1(n\omega) + \frac{2}{L(L+1)}\mathcal{E}_2(n\omega),$$

where $\mathcal{A}_1(n\omega)$ and $\mathcal{E}_2(n\omega)$ are quasi-periodic (and hence bounded) expressions. Note that if $\hat{\gamma}_{e_1} \neq 0$, the new iterates are given by

$$z_n^{(2L,\omega_1,2)} = \hat{\gamma}_{e_1}\mathrm{e}^{\mathrm{i}n\omega_1}(1+\Gamma^{(2L,\omega_1,2)}(n\omega)),$$

where $\Gamma^{(2L,\omega_1,2)} : \mathbb{T}^r \to \mathbb{C}$ verifies $\Gamma^{(2L,\omega_1,2)} = \mathcal{O}(1/L^2)$. Then, as done in (11), we can construct a quasi-periodic signal $\{x_n^{(2L,\omega_1,2)}\}_{n\in\mathbb{Z}}$ on $\mathbb{T}$, but now with a smaller perturbation of the rotation. As we show in Proposition 2.22, if $\omega_0 \approx \omega_1$ we have a similar scenario, at least for L not too large (see Remark 2.12).

Remark 2.17. *Besides motivating the reader, there are several reasons to introduce second order unfolding ($p = 2$) separately from the general case $p > 1$. On the one hand, the asymptotic rate $\mathcal{O}(1/L^2)$ gives a sufficiently good performance. On the other hand, we note that this asymptotic speed is only secured when $\omega_0 = \omega_1$. Hence, any discrepancy between ω_0 and our target frequency is propagated through the unfolding process. The potential disturbance of this discrepancy increases with the extrapolation order. Finally, note that for $p = 2$ we have explicit formulae* (15) *and* (16) *for any general value of L. In higher order extrapolations we restrict to choose L as powers of two in order to obtain simple extrapolation coefficients.*

Remark 2.18. *It is worth mentioning that the term $\mathrm{e}^{\mathrm{i}n\omega_0}$ is included into the definition of $\widetilde{\mathcal{Z}}_n^{(L,\omega_0,2)}$ in* (15) *to simplify the presentation. For practical purposes, it is more efficient to introduce $\mathrm{e}^{\mathrm{i}n\omega_0}$ when defining $z_n^{(2L,\omega_0,2)}$ in* (16)*, thus reducing the amount of operations.*

2.3.3 Unfolding of order p

Given a quasi-periodic signal, we introduce the following higher order averages that extend Definitions 2.10 and 2.16 to any $p \in \mathbb{N}$.

Definition 2.19. *Under the same notations and hypotheses of Definition 2.10, we introduce the recursive sums*

$$\mathcal{Z}_n^{(L,\omega_0,1)} = \sum_{m=n}^{L+n-1} z_m \mathrm{e}^{-\mathrm{i}m\omega_0}, \qquad \mathcal{Z}_n^{(L,\omega_0,p)} = \sum_{l=1}^{L} \mathcal{Z}_n^{(l,\omega_0,p-1)}, \quad p \geq 2, \tag{17}$$

and the averaged sums of order p

$$\widetilde{\mathcal{Z}}_n^{(L,\omega_0,p)} = \left[\binom{N+p-1}{p}^{-1} \mathcal{Z}_n^{(L,\omega_0,p)} \right] \mathrm{e}^{\mathrm{i}n\omega_0}. \tag{18}$$

We take fixed values of $p \geq 1$ and $q \geq p$ and we define the new sequence

$$z_n^{(2^q,\omega_0,p)} = \sum_{j=0}^{p-1} c_j^{(p-1)} \widetilde{\mathcal{Z}}_n^{(L_j,\omega_0,p)}, \tag{19}$$

where $L_j = 2^{q-p+j+1}$ and the (extrapolation) coefficients $c_j^{(m)}$ are given by

$$c_j^{(m)} = (-1)^{m-j} \frac{2^{j(j+1)/2}}{\delta(j)\delta(m-j)}, \qquad \delta(n) = (2^n-1)(2^{n-1}-1)\cdots(2^1-1), \qquad \delta(0) = 1. \tag{20}$$

As before, $\{z_n^{(2^q,\omega_0,p)}\}_{n\in\mathbb{Z}}$ is a quasi-periodic signal with frequency vector ω for most values of ω_0.

Remark 2.20. *Following [30, 36], we select L_j as powers of two in order to give explicit formulae for the extrapolation coefficients. Note that the important thing to perform the extrapolation is that the values of L_j in* (19) *behave geometrically in j, so other choices can be made.*

Remark 2.21. *Sequence $\{z_n^{(2^q,\omega_0,p)}\}$ gives an unfolding of order p of $\{z_n\}$ computed from the approximate frequency ω_0. To define $z_n^{(2^q,\omega_0,p)}$ we are using $L = 2^q$ consecutive iterates z_l, for $l \in \{n, \ldots, n+L-1\}$. As discussed in Proposition 2.22, if ω_0 is close enough to a particular frequency ω_1 and $L|\omega_0 - \omega_1|$ is fairly small, then $z_n^{(2^q,\omega_0,p)}$ is a perturbation of order $\mathcal{O}(1/L^p) = \mathcal{O}(2^{-pq})$ of a rotation of angle ω_1.*

Proposition 2.22. *Assume the same notations and hypotheses of Definition 2.10 and suppose that ω_0 satisfies the Diophantine bounds in* (14)*. Then, there exists an analytic function*

$\gamma^{(2^q,\omega_0,p)}: \mathbb{T}^r \to \mathbb{C}$ *such that the sequence* $z_n^{(2^q,\omega_0,p)}$ *introduced in Definition 2.19 can be written as* $z_n^{(2^q,\omega_0,p)} = \gamma^{(2^q,\omega_0,p)}(n\omega)$ *and it turns out that, for a fixed* p*,*

$$|z_n^{(2^q,\omega_0,p)} - \hat{\gamma}_{e_1}^{(2^q,\omega_0,p)} \mathrm{e}^{\mathrm{i}n\omega_1}| = \mathcal{O}(2^{-pq}), \qquad \forall n \in \mathbb{Z}. \tag{21}$$

Moreover, the Fourier coefficient $\hat{\gamma}_{e_1}^{(2^q,\omega_0,p)}$ *verifies* $\lim_{\omega_0\to\omega_1} \hat{\gamma}^{(2^q,\omega_0,p)} = \hat{\gamma}_{e_1}$*. This limit is uniform on* q *provided that* $2^q|\omega_1 - \omega_0| \to 0$*.*

Proof. This result is a straightforward adaptation of Proposition 2.18 in [30], that essentially follows ideas introduced in [36]. For this reason, we focus on the computational details of the proof, omitting some technical aspects. Specifically, we are referring to the quasi-periodic expressions $\{\mathcal{A}_l^{(\omega_0,p)}\}_{l=1,\dots,p-1}$ and $\mathcal{E}^{(L,\omega_0,p)}$, which are convergent and bounded by a constant c_p (independent of L). By taking into account (14) and the analyticity assumptions on the signal (see Remark 2.5), these claims are clear for any reader familiar with estimates on solutions of small divisors equations. For more details, see [36].

To simplify the notations we set $\varepsilon = \omega_1 - \omega_0$. The cornerstone of the proof are the following expressions, which can be easily obtained by induction:

$$\begin{aligned}
\mathcal{Z}_n^{(L,\omega_0,p)} &= \Delta^{(L,\omega_0,p)} \mathrm{e}^{\mathrm{i}n\varepsilon} + \left(\sum_{l=1}^{p-1} \binom{L+l-1}{l} \mathcal{A}_l^{(\omega_0,p)}(n\omega) + \mathcal{E}^{(L,\omega_0,p)}(n\omega) \right) \mathrm{e}^{-\mathrm{i}n\omega_0}, \\
\widetilde{\mathcal{Z}}_n^{(L,\omega_0,p)} &= \widetilde{\Delta}^{(L,\omega_0,p)} \mathrm{e}^{\mathrm{i}n\omega_1} + \sum_{l=1}^{p-1} \frac{(p-l+1)\cdots p\, \mathcal{A}_l^{(\omega_0,p)}(n\omega)}{(L+p-l)\cdots(L+p-1)} + \frac{p!\, \mathcal{E}^{(L,\omega_0,p)}(n\omega)}{L\cdots(L+p-1)},
\end{aligned}$$

where

$$\begin{aligned}
\mathcal{A}_l^{(\omega_0,p)}(n\omega) &= (-1)^{l+1} \sum_{k\neq e_1} \hat{\gamma}_k \frac{\mathrm{e}^{\mathrm{i}(l-1)(\langle k,\omega\rangle - \omega_0)}}{(1-\mathrm{e}^{\mathrm{i}(\langle k,\omega\rangle-\omega_0)})^l} \mathrm{e}^{\mathrm{i}n\langle k,\omega\rangle}, \\
\mathcal{E}^{(L,\omega_0,p)}(n\omega) &= (-1)^{p+1} \sum_{k\neq e_1} \hat{\gamma}_k \frac{\mathrm{e}^{\mathrm{i}(p-1)(\langle k,\omega\rangle - \omega_0)}(1-\mathrm{e}^{\mathrm{i}L(\langle k,\omega\rangle-\omega_0)})}{(1-\mathrm{e}^{\mathrm{i}(\langle k,\omega\rangle-\omega_0)})^p} \mathrm{e}^{\mathrm{i}n\langle k,\omega\rangle},
\end{aligned}$$

whereas $\Delta^{(L,\omega_0,p)}$ and $\widetilde{\Delta}^{(L,\omega_0,p)}$ are defined recursively by:

$$\Delta^{(L,\omega_0,1)} = \hat{\gamma}_{e_1} \frac{1-\mathrm{e}^{\mathrm{i}\varepsilon L}}{1-\mathrm{e}^{\mathrm{i}\varepsilon}}, \quad \Delta^{(L,\omega_0,p)} = \sum_{l=1}^{L} \Delta^{(l,\omega_0,p-1)}, \quad \widetilde{\Delta}^{(L,\omega_0,p)} = \binom{L+p-1}{p}^{-1} \Delta^{(L,\omega_0,p)}.$$

From these expression it is not difficult to verify that $\lim_{\varepsilon\to 0} \widetilde{\Delta}^{(L,\omega_0,p)} = \hat{\gamma}_{e_1}$. We re-write $\widetilde{\mathcal{Z}}_n^{(L,\omega_0,p)}$ as:

$$\widetilde{\mathcal{Z}}_n^{(L,\omega_0,p)} = \widetilde{\Delta}^{(L,\omega_0,p)} \mathrm{e}^{\mathrm{i}n\omega_1} + \sum_{l=1}^{p-1} \frac{\widetilde{\mathcal{A}}_l^{(\omega_0,p)}(n\omega)}{L^l} + \widetilde{\mathcal{E}}^{(L,\omega_0,p)}(n\omega). \tag{22}$$

Note that the new function-coefficients $\{\widetilde{\mathcal{A}}_l^{(\omega_0,p)}\}_{l=1,\ldots,p-1}$ $\widetilde{\mathcal{A}}_l^{(\omega_0,p)}$ are independent of L and that $\widetilde{\mathcal{E}}^{(L,\omega_0,p)}$ is of $\mathcal{O}(1/L^p)$, so expression (22) is well-suited for Richardson extrapolation. To this end, we compute the averaged sums $\{\widetilde{\mathcal{Z}}_n^{(L_j,\omega_0,p)}\}_{j=0,\ldots,p-1}$ for $L_j = 2^{q-p+j+1}$. Then, a suitable combination of these averaged sums allows removing the coefficients $\{\widetilde{\mathcal{A}}_l^{(\omega_0,p)}\}_{l=1,\ldots,p-1}$. The resulting expression behaves in n as a rotation of angle ω_1 plus a quasi-periodic error of $\mathcal{O}(1/L_0^p)$.

To formalize the construction, we consider a sequence $\{S_L\}_{L\geq 1}$ that satisfies

$$S_L = \alpha + \sum_{j=0}^{p-1} \frac{A_l}{L^l}. \tag{23}$$

In [30, 36] it was shown that $\alpha = \hat{\Theta}^{(p,q)}(\{S_L\})$, where the extrapolation operator $\hat{\Theta}^{(p,q)}$ is defined as

$$\hat{\Theta}^{(p,q)}(\{S_L\}) = \sum_{j=0}^{p-1} c_j^{(p-1)} S_{L_j}, \qquad L_j = 2^{q-p+j+1}, \tag{24}$$

and the coefficients $c_j^{(m)}$ are given in (20). Then, we use (24) for $S_L = \widetilde{\mathcal{Z}}_n^{(L,\omega_0,p)} - \widetilde{\Delta}^{(L,\omega_0,p)} \mathrm{e}^{\mathrm{i}n\omega_1} - \widetilde{\mathcal{E}}^{(L,\omega_0,p)}(n\omega)$ and $\alpha = 0$, thus obtaining

$$z_n^{(2^q,\omega_0,p)} = \gamma^{(2^q,\omega_0,p)}(n\omega) := \underbrace{\sum_{j=0}^{p-1} c_j^{(p-1)} \widetilde{\Delta}^{(L,\omega_0,p)}\, \mathrm{e}^{\mathrm{i}n\omega_1}}_{\hat{\gamma}_{e_1}^{(2^q,\omega_0,p)}} + \sum_{j=0}^{p-1} c_j^{(p-1)} \widetilde{\mathcal{E}}^{(L,\omega_0,p)}(n\omega).$$

Finally, bounds in (21) are straightforward and $\lim_{\varepsilon\to 0} \hat{\gamma}_{e_1}^{(2^q,\omega_0,p)} = \hat{\gamma}_{e_1}$ follows from $\sum_{j=0}^{p-1} c_j^{(p-1)} = 1$. $\square$

Finally, Next we discuss several implementation details in order to help the reader to obtain efficient algorithms to "unfold" a given quasi-periodic signal.

Remark 2.23. *Assume that for some n and L we know $\mathcal{Z}_n^{(L,\omega_0,k)}$, for any $k = 1, \ldots, p$. Then, to obtain $\mathcal{Z}_{n+1}^{(L,\omega_0,k)}$ we do not have to compute the full sums involved in equation* (17), *but just to update the previous n-iterates as follows:*

$$\begin{aligned} \mathcal{Z}_{n+1}^{(L,\omega_0,1)} &= \mathcal{Z}_n^{(L,\omega_0,1)} + z_{L+n}\mathrm{e}^{-\mathrm{i}(L+n)\omega_0} - z_n \mathrm{e}^{-\mathrm{i}n\omega_0}, \\ \mathcal{Z}_{n+1}^{(L,\omega_0,k)} &= \mathcal{Z}_n^{(L,\omega_0,k)} + \mathcal{Z}_{n+1}^{(L,\omega_0,k-1)} - \binom{L+k-2}{k-1} z_n \mathrm{e}^{-\mathrm{i}n\omega_0}, \qquad k = 2, \ldots, p. \end{aligned}$$

These formulae play a major role in the practical implementation of the method. Since definition of $z_n^{(2^q,\omega_0,p)}$ in (19) *only involves the values of $\widetilde{\mathcal{Z}}_n^{(L,\omega_0,p)}$ when $L = L_j$, for $j = 0, \ldots, p-1$, we* *can try to avoid the computation of* $\mathcal{Z}_n^{(L,\omega_0,p)}$ *for* $L \neq L_j$. *But note that if we use the definition of* $\mathcal{Z}_n^{(L_j,\omega_0,p)}$ *in* (17)*, then it involves the sum of* $\mathcal{Z}_n^{(l,\omega_0,p-1)}$ *for any* $l = 1, \dots, L_j$. *Then, we proceed as follows:*

- *Compute "the first iterate"* $\mathcal{Z}_1^{(l,\omega_0,k)}$ *for any* $l = 1, \dots, 2^q$ *and* $k = 1, \dots, p$ *by using the recurrences in* (17).
- *For a given* $n \geq 1$, *use formulae above to compute* $\mathcal{Z}_{n+1}^{(L,\omega_0,k)}$ *for any* $k = 1, \dots, p$, *but only when* $L = L_j$ *for some* $j = 0, \dots, p-1$.

Finally, we also observe that formulae above perform specially fast (in a computer) for $p = 2$, *since then* $\binom{L+p-2}{p-1} = L$ *and we work with values of* L *that are powers of two. Products by two correspond to shifts using binary arithmetics.*

Remark 2.24. *We can reduce the number of products in each extrapolation simply by adding the combinatorial numbers to the coefficients* $c_j^{(p)}$. *Specifically,*

$$z_n^{(2^q,\omega_0,p)} = \sum_{j=0}^{p-1} \tilde{c}_j^{(p-1)} \mathcal{Z}_n^{(L_j,\omega_0,p)}, \qquad \tilde{c}_j^{(p-1)} = c_j^{(p-1)} \binom{L_j+p-1}{p}^{-1},$$

where $\tilde{c}_j^{(p-1)}$ *can be computed at the beginning of the process (although now they depend on the prefixed* q *through* $L_j = 2^{q-p+j+1}$*).*

2.4 Computation of frequencies

In this section we sketch the method developed in [36] for computing Diophantine rotation numbers of circle diffeomorphisms. Besides for the sake of completeness, the main motivation for including this reviewing in the paper is to show that the construction is also well-suited to deal with quasi-periodic signals on the circle depending on many frequencies. Indeed, in this presentation we omit any reference to maps on the circle. As noted before, existence or not of such a map in connexion to a projected signal on $\mathbb{T}$ is not necessary for our purposes. This methodology, applied to the unfolded signal constructed in Section 2.3, constitutes the cornerstone of our approach to the computation of frequencies. We do not plan to perform a systematic presentation of the methodology nor to discuss its full theoretical justification. For details we refer to [36].

The starting point of the method is a quasi-periodic signal on $\mathbb{T}$ whose lift to $\mathbb{R}$ takes the form

$$x_n = n\omega_1 + \phi(\omega\theta) = n\omega_1 + \sum_{k\in\mathbb{Z}^r} \hat{\phi}_k e^{i\langle k,\omega\rangle}, \qquad n \in \mathbb{N}, \tag{25}$$

where $\phi : \mathbb{T}^r \to \mathbb{R}$. This means that ω_1, which is our target, is the frequency of the signal that leads the rotation. Notice that we are not assuming that (25) is related to any kind of map or quasi-periodically forced map on the circle. In analogy with the definition of the rotation number of circle maps, we have that $\omega_1 = \lim_{n\to\infty}(x_n - x_0)/n$, for which we expect a convergence rate of $\mathcal{O}(1/n)$. Note that this rate is not satisfactory for practical purposes since it requites to compute a tremendous number of iterates in order to reach a moderate tolerance. Again, in a complete analogy with Definition 2.19, the key issue for accelerating the convergence speed of ω_1 is to introduce suitable recursive and averaged sums.

Definition 2.25. *Given a sequence $\{x_n\}_{n\geq 1}$, we introduce the following recursive sums:*

$$S_N^{(0)} = x_N, \quad S_N^{(p)} = \sum_{n=1}^{N} S_n^{(p-1)}, \qquad N, p \geq 1,$$

and the following averaged sums of order p:

$$\widetilde{S}_N^{(p)} = \binom{N+p}{p+1}^{-1} S_N^{(p)}.$$

Remark 2.26. *The combinatorial numbers in the definition of $\widetilde{S}_N^{(p)}$ are not the same as those in the definition of $\widetilde{\mathcal{Z}}_n^{(L,\omega_0,p)}$ in* (18). *This is because the leading term of x_n in* (25) *is of $\mathcal{O}(n)$ while the term $\hat{\gamma}_1 \mathrm{e}^{\mathrm{i}n\omega_1}$ that we want to extrapolate from z_n in* (1) *is of $\mathcal{O}(1)$. This discrepancy between the "dominant orders" is also evident in the expressions of the corresponding extrapolation operators (compare* (23) *and* (24) *with* (27)*).*

Proposition 2.27. *Let us consider a real-valued signal $\{x_n\}_{n\in\mathbb{N}}$ of the form* (25)*. We assume that ϕ is analytic and that the vector $\omega \in \mathbb{R}^r$ verifies Diophantine conditions* (2)*. Then, we have the following expression for the averaged sums of Definition 2.25:*

$$\widetilde{S}_N^{(p)} = \omega_1 + \sum_{l=1}^{p} \frac{\widetilde{A}_l^{(p)}(n\omega)}{N^l} + \widetilde{E}^{(N,p)}(n\omega), \qquad N \geq 1, \tag{26}$$

where $\{\widetilde{A}_l^{(p)}(n\omega)\}$ and $\widetilde{E}^{(N,p)}(n\omega)$ are analytic and quasi-periodic expressions, with $\widetilde{E}^{(N,p)} = \mathcal{O}(1/N^{p+1})$. Specifically, $|\widetilde{E}^{(N,p)}| \leq C_p/N^{p+1}$, for some $C_p > 0$.

Furthermore, we consider fixed integer values $q \geq p \geq 1$ and we define the following extrapolation operator of order p, which involves $N = 2^q$ consecutive iterates of $\{x_n\}_{n\in\mathbb{N}}$

$$\Theta^{(p,q)} = \sum_{j=0}^{p} c_j^{(p)} \widetilde{S}_{N_j}^{(p)}, \tag{27}$$

where $N_j = 2^{q-p+j}$ and the coefficients $c_j^{(p)}$ are given in (20)*. Then, we have*

$$\omega_1 = \Theta^{(p,q)} + e(p,q), \tag{28}$$

where $e(p,q) = \mathcal{O}(1/N^{p+1}) = \mathcal{O}(2^{-(p+1)q})$.

We omit the proof of Proposition 2.27 because this result is obtained by following the same lines as in the proof of Proposition 2.22. As done in Definition 2.19 (see Remark 2.20), we follow [36, 30] and select N_j as powers of two. Of course, other choices of N_j (behaving geometrically in j) can be considered —and it may be even recommended depending on the problem. Then, the extrapolated value for ω_1 follows just by solving a $(p+1)\times(p+1)$ linear system of equations.

Remark 2.28. *Since $e^{(p,q)}$ behaves as $|e^{(p,q)}| \approx C_p 2^{-(p+1)q}$, we can try to estimate the value of C_p by means of two extrapolated values of order p, say $\Theta^{(p,q)}$ and $\Theta^{(p,q-1)}$. As we expect $\Theta^{(p,q)}$ to be closer to ω_1 than $\Theta^{(p,q-1)}$, we estimate C_p by considering formula* (28) *for $q-1$ and then replacing ω_1 by $\Theta^{(p,q)}$. We obtain the following heuristic estimate (see [36]):*

$$|e^{(p,q)}| \approx 2^{-(p+1)}\nu|\Theta^{(p,q)} - \Theta^{(p,q-1)}|, \tag{29}$$

where ν is a "safety parameter" to prevent the fact that C_p can oscillate as a function of q.

Remark 2.29. *Note that the averaging order p and the exponent q in the number of iterates in the definition of $\Theta^{(p,q)}$ in* (27) *have nothing to do with their counterparts in the definition of the unfolded signal $z_n^{(2^q,\omega_0,p)}$ in* (19). *Indeed, the selection of suitable values of p and q in the extrapolation of the frequency is independent on how the signal has been unfolded.*

Remark 2.30. *If the signal comes from experimental data, then it is natural to assume that it contains some round off errors that behave in random way. Such situation was discussed in [30], where the uncertainty coming from experimental data was simulated by adding to a quasi-periodic signal (with just one frequency) a normally distributed random error. The result was that the presented methodology still provides very accurate approximations to the frequency of the signal, significantly smaller than the size of the random component.*

Remark 2.31. *In [30] the methodology of [36] for computing rotation numbers was addressed in order to calculate derivatives of the rotation number with respect to parameters. Although this issue is not discussed in this paper, this approach can be adapted to the framework of the frequency analysis.*

2.5 Computation of amplitudes

In a very naive way, the unfolding construction presented in Section 2.3 basically tries to extrapolate the Fourier harmonic corresponding to the "closest frequency" to ω_0. Once we have computed a refined value for the approximate frequency ω_0, we can adapt the construction to get a posteriori the corresponding amplitude by means, again, of averaging and extrapolation. We emphasize that this procedure does not require any information on the remaining frequencies.

Proposition 2.32. *With the same notations and hypotheses of Definition 2.10. Let $k^* \in \mathbb{Z}^r$ and $\omega^* = \langle k^*, \omega\rangle$ (i. e., ω^* is the combination of the basic frequencies $\omega \in \mathbb{R}^r$ associated to the*

Fourier coefficient $\hat{\gamma}_{k^*}$ in (1)*). We introduce the following recursive and averaged sums for the quasi-periodic signal $\{z_n\}$, for any $N, p \geq 1$,*

$$\mathcal{F}_N^{(k^*,0)} = z_N \mathrm{e}^{-\mathrm{i}N\omega^*}, \quad \mathcal{F}_N^{(k^*,p)} = \sum_{n=1}^{N} \mathcal{F}_n^{(k^*,p-1)}, \quad \widetilde{\mathcal{F}}_N^{(k^*,p)} = \binom{N+p-1}{p}^{-1} \mathcal{F}_N^{(k^*,p)}.$$

Furthermore, given integer values $q \geq p \geq 1$, we define the following extrapolation operator of order p, which involves $N = 2^q$ consecutive iterates of $\{z_n\}$:

$$\Gamma^{(k^*,p,q)} = \sum_{j=0}^{p-1} c_j^{(p-1)} \widetilde{\mathcal{F}}_{L_j}^{(k^*,p)}, \tag{30}$$

where $L_j = 2^{q-p+j+1}$ and the coefficients $c_j^{(p-1)}$ are given in (20)*. Then, we have*

$$\hat{\gamma}_{k^*} = \Gamma^{(k^*,p,q)} + e(k^*, p, q),$$

where $e(k^*, p, q) = \mathcal{O}(1/N^p) = \mathcal{O}(2^{-pq})$.

Justification of Proposition 2.32 follows by the same arguments as Propositions 2.22 and 2.27 (see [30] for the case of a single frequency signal).

Remark 2.33. *Once a frequency is known, formula* (30) *allows computing its Fourier coefficient with high accuracy at a moderate cost. We observe that we can estimate the commited error in the same way as in Remark 2.28. Specifically,*

$$|e(k^*, p, q)| \approx 2^{-p}\nu|\Gamma^{(k^*,p,q)} - \Gamma^{(k^*,p,q-1)}|.$$

Remark 2.34. *Note that although Proposition 2.32 is formulated in terms of a single amplitude, it can be performed simultaneously for multiple Fourier coefficients in the spirit of FFT strategies. This allows to save many operations when computing the Fourier representation of the signal.*

In practice, we notice that some problems may arise when computing $\hat{\gamma}_{k^*}$ for large values of k^*. This is not only because the smallness of $\hat{\gamma}_{k^*}$ makes difficult to obtain a significant expression for it, but also because the disturbing effect of the dominant Fourier coefficients of the signal is present along the averaging-extrapolation process. So, although (30) provides a numerical value for $\hat{\gamma}_{k^*}$ with an error of $\mathcal{O}(2^{-pq})$, such result follows after many cancellations between expressions of size larger than $\hat{\gamma}_{k^*}$. This leads to the loss of many significant digits. Hence, if a very accurate Fourier representation of $\{z_n\}$ is needed, one can try to combine Proposition 2.32 with the collocation methods of [13, 14] already mentioned in the introduction. This allows to refine amplitudes and frequencies by the Newton method. Furthermore, sometimes the iterates $\{z_n\}$ correspond to an initial condition giving an approximation of an invariant torus of a Hamiltonian system or symplectic map. Then, in the literature there are "non-perturbative" KAM methods proving existence of quasi-periodic solutions close to a good enough candidate (see for example [7, 15, 31]). Then, after computing the approximate frequencies and amplitudes for $\{z_n\}$, we can correct them by means of these KAM schemes.

Besides the pure computation of the Fourier coefficients, the following remarks account for some interesting applications of Proposition 2.32.

Remark 2.35. *As noted in Remark 2.15, if the unfolding is not performed correctly, it can happen that the refinement of a frequency (algorithm described in Section 2.4) converges to a number $\bar{\omega}_1$ which is not a frequency of the original signal. Indeed, we only can claim that $\bar{\omega}_1$ is the rotation frequency around the origin of the partially unfolded signal. In general, we can easily realize about this failure due to a big discrepancy between the approximate frequency ω_0 and $\bar{\omega}_1$. A systematic way to check the correctness of $\bar{\omega}_1$ is to apply Proposition 2.32 with $\omega^* = \bar{\omega}_1$. If $\bar{\omega}_1$ is a true frequency, then we end up by computing the corresponding Fourier coefficient. If $\bar{\omega}_1$ is not a frequency, we expect that the extrapolated amplitude tends to zero very quickly.*

Remark 2.36. *The simplest but perhaps most interesting case of Proposition 2.32 is for $k^* = 0$. Note that $\hat{\gamma}_0$ corresponds to the average of the quasi-periodic signal, which can be computed without any information on the frequencies. Let us observe that the computational cost of $\hat{\gamma}_0$ is fairly less expensive than of any other Fourier coefficient (there is no trigonometric part involved in the computations). We have the following straightforward applications:*

(a) Generically, $\hat{\gamma}_0$ is one of the largest Fourier coefficients of the signal. If we subtract $\hat{\gamma}_0$ to the signal, then we can improve the unfolding process.

(b) The study of the convergence of $\Gamma^{(0,p,q)}$ in (30) *can be used as a fast indicator to decide if a given orbit is quasi-periodic or not before performing frequency analysis. Note that fast convergence does not always means that the signal is quasi-periodic (for instance, this criteria also detects initial conditions belonging to the stable manifold of an invariant torus). Moreover, divergence of $\Gamma^{(0,p,q)}$ (including oscillatory behaviour) or even slow convergence, means that the signal is not quasi-periodic (or, at least, that has bad Diophantine frequencies).*

2.6 First approximation of frequencies

As explained in the Introduction, the classical method to obtain approximations of the frequencies of a quasi-periodic signal is to look for the peaks of the modulus of the discrete Fourier transform (DFT) of the studied signal. As we have already mentioned, this approach may be refined by introducing suitable window functions on the DFT or by means of collocation methods, although the practical implementation of any of both approaches forces to compute simultaneously the amplitudes of the signal.

The unfolding methodology presented in this paper requires approximations of the frequencies (but not of the corresponding amplitudes). Sometimes these approximations are given by the context. For example, if we are in a neighbourhood of an elliptic fixed point or carrying out a continuation with respect to parameters of a quasi-periodic solution with known frequencies. In Section 3 we study a (large) neighborhood of an elliptic equilibrium point of a Hamiltonian system and we include quasi-periodic perturbations. In this case, one can perform a continuation process for the frequencies starting close to the equilibrium point. Otherwise, we can obtain approximations to the frequencies by a preliminary study of the signal by a DFT-based method (performed with low accuracy).

Besides, we have the chance of adapting the unfolding methodology of Section 2.3 in order to get such approximations. Next, we outline the main lines of this approach, which can be understood as an alternative to the use of filters in the DFT. We refer to [30] for the case of a single frequency and for the accurate description of some implementation details.

Let us consider a quasi-periodic signal $\{z_n\}$. From a sample of L points we compute its DFT as a function of ω_0, given by the formula

$$\omega_0 \longmapsto \frac{1}{L}\sum_{m=0}^{L-1} z_m \mathrm{e}^{-\mathrm{i}m\omega_0}. \tag{31}$$

Note that this expression coincides with the "zero iterate" $z_0^{(L,\omega_0)}$ of the unfolded signal (8) of order $p = 1$. We denote $Z^{(L,1)}(\omega_0) = |z_0^{(L,\omega_0)}|$ the modulus of (31). The classical approach to the frequency analysis is based on the following observation. Assume for the moment that $\{z_n\}$ is a quasi-periodic signal consisting of a single Fourier harmonic, say $z_n = \mathrm{e}^{\mathrm{i}n\omega_1}$. Then, the modulus of the DFT is given by

$$Z_0^{(L,1)}(\omega_0) = \frac{1}{L}\left|\frac{\sin(L(\omega_1-\omega_0)/2)}{\sin((\omega_1-\omega_0)/2)}\right|, \tag{32}$$

that has a local maximum at $\omega_0 = \omega_1$. If $\{z_n\}$ is a generic (but smooth enough) quasi-periodic signal, then the effect of the remaining Fourier harmonics on $Z^{(L,1)}(\omega_0)$ can be viewed as a perturbation of (32) around $\omega_0 = \omega_1$. This leads to a displacement of the maximum of $Z_0^{(L,1)}(\omega_0)$, which allows computing a "dominant" frequency ω_1 of $\{z_n\}$ with an accuracy of $\mathcal{O}(1/L)$. As we already summarized in the introduction, this displacement can be modulated by introducing suitable window functions in the DFT.

Here, we propose a new approach to correct the DFT, based on higher order unfoldings. Let us concentrate on the case $p = 2$. Specifically, we consider a sample of $2L$ points of $\{z_n\}$ and introduce $Z^{(2L,2)}(\omega_0) = |z_0^{(2L,\omega_0,2)}|$, where $z_0^{(2L,\omega_0,2)}$ is the zero iterate of the unfolded signal (see Definition 2.16). If $z_n = \mathrm{e}^{\mathrm{i}n\omega_1}$, then it is not difficult to realize that the corresponding module function, namely $Z_0^{(2L,2)}(\omega_0)$, also reaches a local maximum at $\omega_0 = \omega_1$. As shown in Figure 3, the resolution of this maximum for $Z_0^{(2L,2)}(\omega_0)$ is magnified with respect to $Z_0^{(2L,1)}(\omega_0)$, in the sense that the spurious peaks nearby are modulated by the unfolding. We recall that when

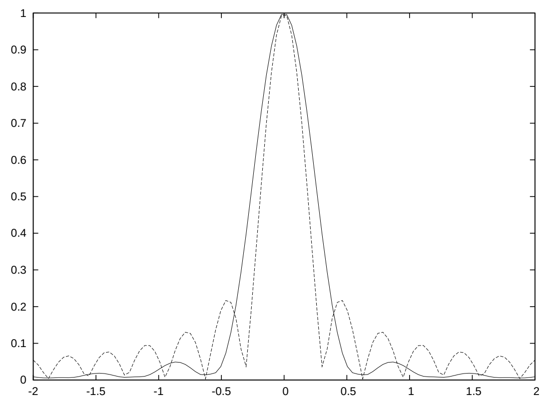

Figure 3: Comparison between $Z_0^{(2L,2)}(\omega_0)$ (continuous graph) and $Z_0^{(2L,2)}(\omega_0)$ (discontinuous graph) for $L = 10$. We plot these modulus functions in terms of $\omega_1 - \omega_0$, so the wanted local maximum is set at the origin.

$\omega_0 \approx \omega_1$ are close enough (see Remark 2.21), then the unfolded signal "tends to" the planar rotation $\mathrm{e}^{\mathrm{i}n\omega_1}$ with a convergence rate of $\mathcal{O}(1/L^2)$ (see Proposition 2.22). This implies that from the study of $Z^{(2L,2)}(\omega_0)$ we can determine a dominant frequency ω_1 of $\{z_n\}$ up to an accuracy of $\mathcal{O}(1/L^2)$. Furthermore, we can extend this construction up to an arbitrary order p considering $Z^{(2^q,p)}(\omega_0) = |z_0^{(2^q,\omega_0,p)}|$ (see Definition 2.19). With this definition, the theoretical resolution of the maximum improves up to $\mathcal{O}(2^{-pq})$ (see Proposition 2.22).

To built a refined methodology to detect frequencies based on the study of the maxima of $Z^{(2^q,p)}(\omega_0)$ is not the purpose of this work (this is the spirit of [25, 13]) although in this way we have the chance of developing a self-contained toolkit to perform frequency analysis. In this sense, we remark that to deal with $Z^{(2^q,p)}(\omega_0)$ has some advantages with respect to introduce filters on the DFT, both from the point of view of dynamics and of regularity. For example, we recall that if we introduce a Hanning filter on the DFT, then we are turning any analytic quasi-periodic signal into a periodic one, with a regularity that depends on the order of the filter. In this way, the Fourier coefficients of the filtered signal behave asymptotically as an inverse power of the order of the coefficient. By contrast, the unfolding procedure of this paper keeps both the analyticity and quasi-periodicity of the signal. In particular, we are not introducing spurious frequencies due to the length of the selected sample. Moreover, if $\omega_0 \approx \omega_1$, then we expect the contribution to $Z^{(2^q,p)}(\omega_0)$ of the high order Fourier harmonics to be exponentially small with respect to the order.

2.7 Testing the method with a known quasi-periodic signal

In this section we test the performance of the methods in an example with known frequencies. Let us consider a quasi-periodic signal $z_n = \gamma(\omega n)$, with three independent frequencies, given

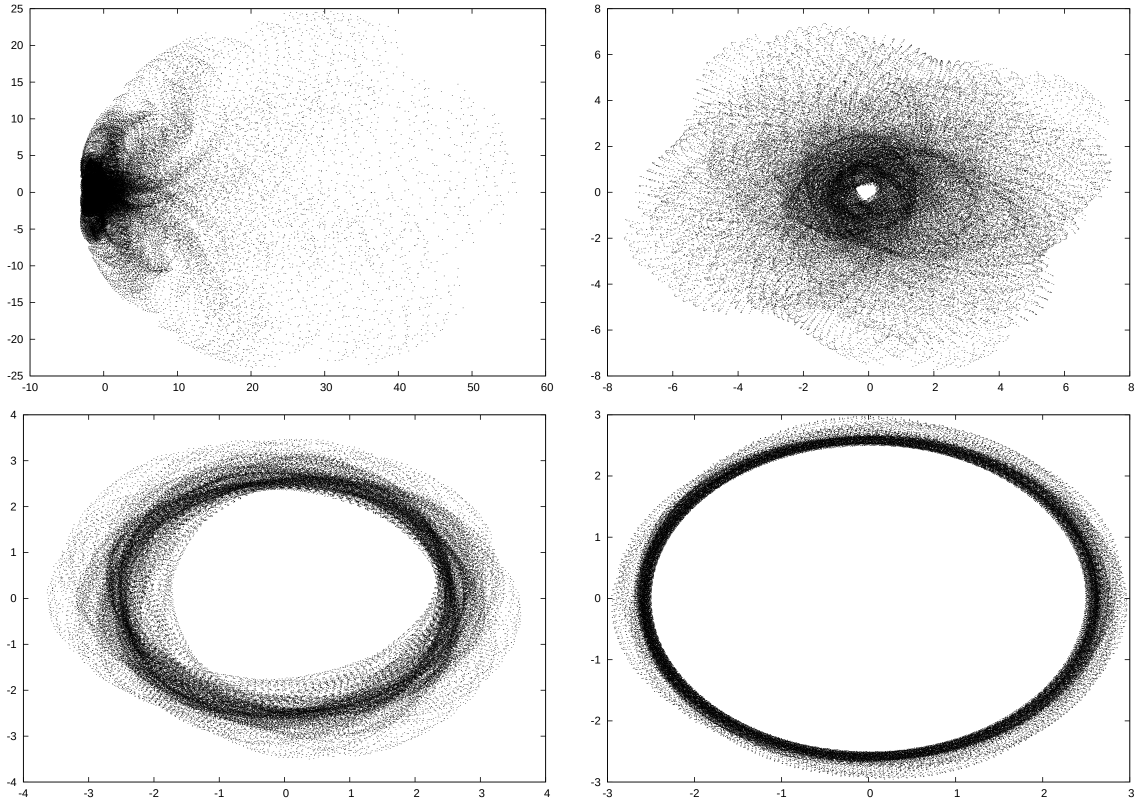

Figure 4: We show 10^5 iterates of the quasi-periodic signal defined by (33) (top-left plot) and the corresponding unfolded signals $\{z_n^{(L,\omega_1)}\}$ using $L = 8$ (top-right plot), $L = 32$ (bottom-left plot) and $L = 128$ (bottom-right plot).

by

$$\gamma(\theta_1, \theta_2, \theta_3) = \frac{\mathrm{e}^{\mathrm{i}\theta_1} + \mathrm{e}^{\mathrm{i}\theta_2} + \mathrm{e}^{\mathrm{i}\theta_3} + \mathrm{e}^{\mathrm{i}(\theta_1+\theta_2)} + \mathrm{e}^{\mathrm{i}(\theta_2+\theta_3)} + \mathrm{e}^{\mathrm{i}(\theta_1-\theta_3)} + \mathrm{e}^{3\mathrm{i}\theta_1}}{(1-\mu\cos(\theta_1))(1-\mu\cos(\theta_2))(1-\mu\cos(\theta_3))}, \tag{33}$$

where $\omega_1 = 2\pi(\sqrt{2}-1)$, $\omega_2 = 2\pi(\sqrt{3}-1)$ and $\omega_3 = \pi(\sqrt{5}-1)$. Taking $\mu \neq 0$ allows to introduce infinitely many harmonics and to break the entiere character of the signal. From the qualitative viewpoint, results do not depend on the particular value of $0 < \mu < 1$, so we take $\mu = 0.3$ in all the computations. Notice that if $\mu \to 1$, then the strip of analyticity of $\gamma(\theta)$ around $\theta \in \mathbb{T}^3$ collapses on the real torus. The reader interested in the behaviour of averaging-extrapolation methods outside their domain of validity is referred to [8, 37].

Some iterates of (33) are shown in Figure 4. We also plot the corresponding first order unfolded signals $\{z_n^{(L,\omega_0)}\}$ (see Definition 2.10), computed in terms of the exact frequency $\omega_0 = \omega_1$ and for $L = 8, 32$ and 128. We observe how the cloud of points of the original signal, that fills up densely an open set of the plane, approaches (as L increases) to a more organized distribution of points on an annulus.

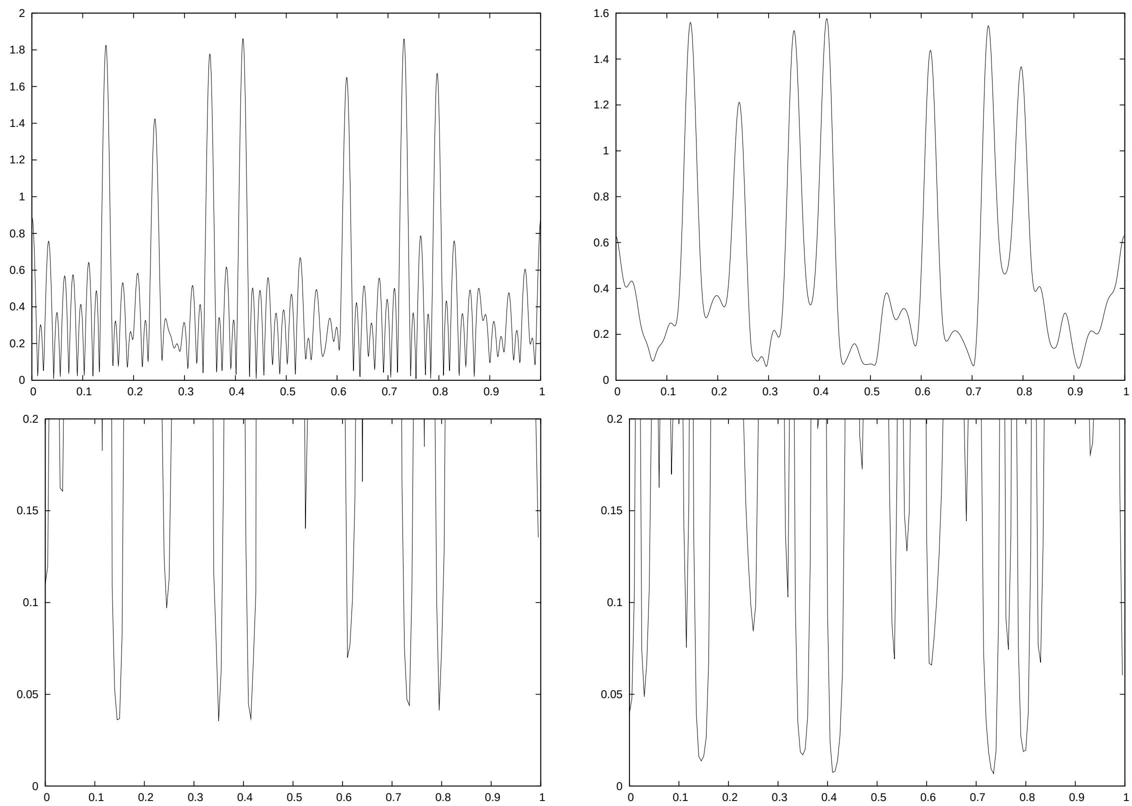

Figure 5: Top: we plot $\frac{\omega_0}{2\pi} \in [0,1] \mapsto Z^{(64,p)}(\omega_0)$ for $p = 1$ (left plot) and $p = 2$ (right plot). Bottom: we plot the standard deviation of the radius for the first 50000 unfolded iterates $z_n^{(2^6,\omega_0,p)}$ as a function of $\frac{\omega_0}{2\pi} \in [0,1]$ for $p = 1$ (left plot) and $p = 2$ (right plot).

Let us illustrate how we can obtain a first guess for the frequencies using the method presented in Section 2.6. Hence, we assume for the moment that the iterates $\{z_n\}$ are know, but that the frequencies of the signal are unknown. We must stress that here we are more interested in illustrating the observed phenomena rather than in describing an efficient and fast implementation of the algorithm. In the top of Figure 5 we show the function $\frac{\omega_0}{2\pi} \mapsto Z^{(L,p)}(\omega_0)$ for $p = 1$ (left plot) and $p = 2$ (right plot) using only $L = 64$ (in the plots frequencies are represented modulo one rather than modulo 2π). The main peaks observed are candidates to approximations to the frequencies of the signal. Observe that for $p = 2$ the number of spurious peaks is significantly reduced. For example, if we compute $\mapsto Z^{(64,2)}(\omega_0)$ for a sample of 200 points $\frac{\omega_0}{2\pi} \in [0,1]$ (with step 0.005), then the obtained numerical approximations for the picks are easy to relate to combinations of the basic frequencies of (33). Indeed, $0.415 \simeq \frac{1}{2\pi}\omega_1$, $0.730 \simeq \frac{1}{2\pi}\omega_2$ and $0.620 \simeq \frac{1}{2\pi}\omega_3$. Another relevant peaks are, for example, $0.145 \simeq \frac{1}{2\pi}(\omega_1 + \omega_2)$, $0.24 \simeq \frac{1}{2\pi}3\omega_1$, $0.350 \simeq \frac{1}{2\pi}(\omega_2 + \omega_3)$ and $0.795 \simeq \frac{1}{2\pi}(\omega_1 - \omega_3)$.

We recall that $Z^{(L,p)}(\omega_0)$ gives the modulus of the zero unfolded iterate computed in terms

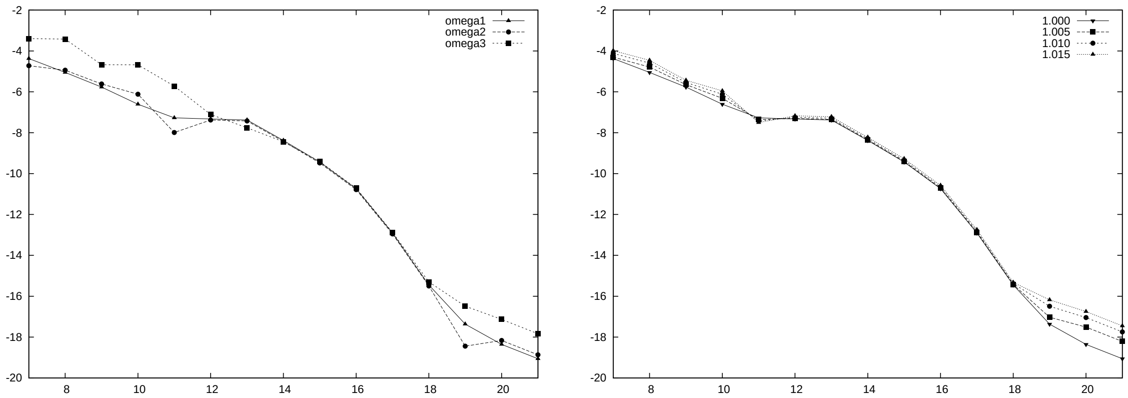

Figure 6: Left: we plot the $\log_{10}$ of the error in the refinement of the frequencies ω_1, ω_2 and ω_3 of (33) (vertical axis) versus q (horizontal axis), where 2^q is the number of used iterates. See the text for details. Right: the same refinement process, now only for the frequency ω_1, by using different approximations $\omega_0 \simeq \omega_1$ to unfold the signal. We take $\omega_0 = \delta\omega_1$, with $\delta = 1, 1.005, 1.01$ and 1.015.

of the approximate frequency ω_0. Hence, $Z^{(L,p)}(\omega_0)$ is useful to detect approximations to the frequencies, but does not show the dynamical features of the unfolding. Now, we illustrate the behaviour of the unfolding process in connection with the peaks of $\frac{\omega_0}{2\pi} \mapsto Z^{(64,p)}(\omega_0)$. The aim is to characterize the phenomenology displayed in Figure 4 in a systematic way. Indeed, for a given ω_0, we compute 50000 iterates of the unfolded signal $\{z_n^{(2^6,\omega_0,p)}\}$ (see Definition 2.19) and we estimate the distance to a circle around the origin by the standard deviation of its averaged radius. Results as function of $\frac{\omega_0}{2\pi} \in [0,1]$ are shown at the bottom of Figure 5 for $p = 1$ (left plot) and $p = 2$ (right plot). In this way, we illustrate how the unfolded process is successful when ω_0 approaches to a frequency of the signal.

Finally, we perform a refinement of the approximated frequencies of the signal (33) using the method described in Section 2.4. Computations are performed using an arithmetic of 32 decimal digits. Specifically, to define the unfolded iterates $\{z_n^{(2^q,\omega_0,p)}\}$ we take $p = 2$ and $q = 6$. To refine the frequency, we select averaging order $p = 3$ and we compute up to $N = 2^{21}$ iterates of the unfolded signal $\{z_n^{(64,\omega_0,2)}\}$. Then, we extrapolate the frequency according to $\Theta^{(p,q)}$ in (27), by using all the possible values of q, i. e., for $3 \leq q \leq 21$. In the left plot of Figure 6 we show the real error in the extrapolation of the basic frequencies ω_1, ω_2 and ω_3, taking ω_0 as the exact value of the frequency to be computed. For $q = 21$ we get almost 20 correct digits. In the right plot of Figure 6 we repeat the computations for the frequency ω_1, now using different approximations ω_0 to unfold the curve. Specifically, we take $\omega_0 = \delta\omega_1$, with $\delta = 1$, 1.005, 1.01 and 1.015. We observe that the results do not depend essentially on the selected value of ω_0, and that the approximation $\frac{\omega_1}{2\pi} \simeq 0.415$, previously obtained looking at the peaks of $Z^{(64,2)}(\omega_0)$, belongs to the interval containing the selected values of ω_0, i. e., $\sqrt{2} - 1 \leq \frac{\omega_0}{2\pi} \leq 1.015 \times (\sqrt{2} - 1)$.

3 Study of a Restricted Three Body Problem

Let us consider two punctual masses (usually called primaries) which move in a circular orbit around their common center of mass according to the Kepler laws. The restricted three body problem (RTBP) describes the motion of a third particle (asteroid) on the vector field produced by these two primaries, assuming that the mass of the asteroid is so small that it does not affect the motion of the first two masses. As usual, we choose units of distance, time, and mass such that the gravitational constant is 1, the period of the primaries is 2π, and the sum of masses of the primaries is 1. With these units the distance between the primaries is also equal to 1. We denote by μ the mass of the smallest primary, $\mu \in (0, \frac{1}{2}]$. In what follows we take $\mu = 0.95388118036309677 \times 10^{-3}$, which corresponds to the Sun-Jupiter system, although the following presentation is common for any μ. For details, see [40].

It is also usual to use a rotating (also called synodic) coordinate system with origin at the center of mass of the primaries, so that the two primaries are kept fixed on the x-axis. The x-axis points to the biggest primary, the z-axis points to the direction of angular motion of the primaries with respect to the center of mass and the y-axis is defined such that we obtain an orthogonal, positive-oriented, system of reference. In this system, the primary of mass μ is at the point $(\mu - 1, 0, 0)$ and the one of mass $1 - \mu$ is at $(\mu, 0, 0)$. Defining momenta $p_x = \dot{x} - y$, $p_y = \dot{y} + x$ and $p_z = z$, the equations of motion can be written in Hamiltonian form, with Hamilton function

$$H_0(x, y, z, p_x, p_y, p_z) = \frac{p_x^2 + p_y^2 + p_z^2}{2} + yp_x - xp_y - \frac{1-\mu}{r_S} - \frac{\mu}{r_J}, \tag{34}$$

where

$$r_S^2 = (x - \mu)^2 + y^2 + z^2, \qquad r_J^2 = (x - \mu + 1)^2 + y^2 + z^2.$$

This system has five equilibrium points belonging to the xy plane. Three of them (the Eulerian points L_1, L_2, and L_3) are on the x axis, and the other two (the Lagrangian points L_4 and L_5) form an equilateral triangle with the primaries. The equilibrium point L_5 is

$$x = \mu - \frac{1}{2}, \quad y = \frac{\sqrt{3}}{2}, \quad z = 0, \quad p_x = -\frac{\sqrt{3}}{2}, \quad p_y = -\frac{1}{2} + \mu, \quad z = 0.$$

As the mass parameter of the Sun-Jupiter system is less than the Routh critical value $\mu_R \simeq 0.03852$, then the point L_5 is linearly stable, with frequencies

$$\omega_1 = \left[\frac{1}{2}(1 - (1 - 27\mu(1-\mu))^{1/2}\right]^{1/2}, \quad \omega_2 = \left[\frac{1}{2}(1 + (1 - 27\mu(1-\mu))^{1/2}\right]^{1/2}, \tag{35}$$

and $\omega_3 = 1$ (this last one corresponds to the vertical oscillations). KAM theory can be applied in a straightforwad (see [9, 22]), thus obtaining plenty of invariant tori close to L_5. The validity of the classical KAM approach applies only in a small neighborhood of the point, meanwhile the stability domain around L_5 is known to be much larger (pioneer results where presented in [34] for the Earth-Moon system). We mean for example to the region of Trojan asteroids (see the studies in [5, 11, 12, 13, 35]). The point L_4 is equivalent.

Our aim is to apply the methodology developed in Section 2 to compute frequencies in the stability domain of L_5. We first consider in Section 3.1 the planar RTBP, where the motion of the asteroid is restricted to the plane of the primaries, i. e., $z = 0$ and $p_z = 0$. In Section 3.2 we deal with the full spatial problem given by (34). Finally, in Section 3.3, we consider the so-called multicircular problem. This system is defined by adding to the RTBP the perturbation of planets moving in circular orbits around the center of mass of the Sun and Jupiter. The Hamiltonian for this perturbed problem, considering d additional planets of masses m_i, orbital radii a_i, and rotation frequencies $\hat{\omega}_i$, with $i = 1, \ldots, d$, is given by

$$H_{MC}(x, y, z, p_x, p_y, p_z, t) = H_0(x, y, z, p_x, p_y, p_z) - m_i \sum_{i=1}^{d} \left(\frac{1}{r_i} + \frac{x \cos\theta_i}{a_i^2} - \frac{y \sin\theta_i}{a_i^2} \right), \quad (36)$$

where $\theta_i = \hat{\omega}_i t + \theta_i^{(0)}$ and

$$r_i^2 = (x - a_i \cos\theta_i)^2 + (y + a_i \sin\theta_i)^2 + z^2.$$

As it is considered in [20], in the computations presented we take into account the gravitational effect of Saturn, Uranus, Neptune, and the Earth.

Remark 3.1. *To numerically integrate the vector fields, we use a high order Taylor method (the order depending on the desired precision). Taylor is very efficient to perform both long term and high accurate computations (to the extend that the use of explicit methods is a suitable choice). Although we coded our own integrator for the problem, very efficient packages have been developed to this purpose and are available to the public (see [2, 24]).*

Remark 3.2. *Using the Taylor method we can integrate the vector field with a large time step —limited by the radius of convergence of the Taylor expansion of the solution. It can happen that the sampling time T used to built a quasi-periodic signal (see Remark 2.7) is smaller than the estimated radius of convergence of the series. In this case, we can save a significant computational time by evaluating the computed Taylor polynomial (also called jet) of the solution as long as we are inside the domain of convergence. Only when this evaluation is not possible, we must re-compute the Taylor expansion. For example, in the planar RTBP, a typical value for the radius of convergence is $h \simeq 1.4$, that is significantly large than reasonable sampling times (we recall that $h = 2\pi$ corresponds to a rotation of Jupiter).*

3.1 Planar case

Next we test the methodology of Section 2 by performing the frequency analysis of initial conditions on the region of stability of L_5. This problem has been already studied in [13]

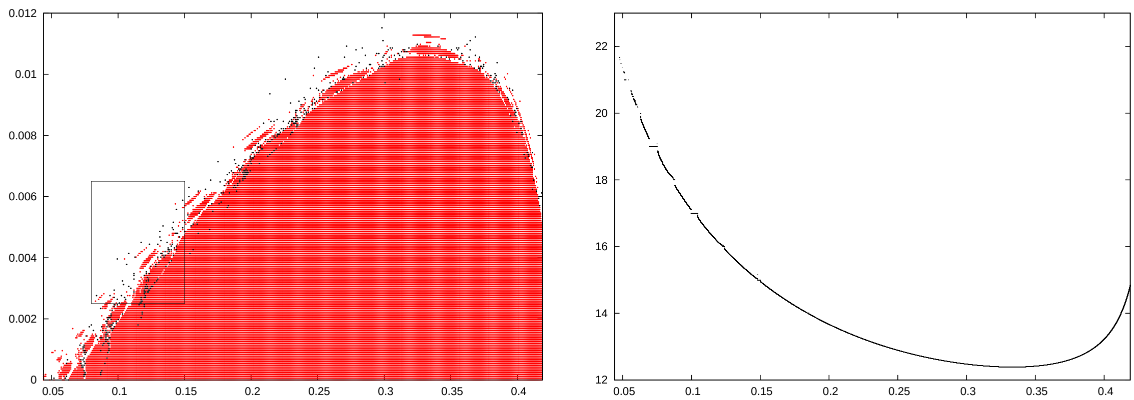

Figure 7: Left: We plot ρ (vertical axis) versus α (horizontal axis) for the initial conditions (38) according to the following criteria: white for those points that escape before $t_{\max} = 66560$, black if the estimated error for the computed frequencies is larger than $6 \cdot 10^{-6}$, and red otherwise. Points within the marked rectangle will be considered again in Figure 12. Right: We show the graph $\omega_1/2\pi$ versus α when $\rho = 0$ only for those points with a final error for the frequencies smaller than 10^{-6}.

using collocation methods so it represents a nice test for the approach presented in this paper. Note that the planar problem has two degrees of freedom so, under isoenergetic non-degeneracy KAM conditions, invariant tori play the role of barriers in phase-space. Indeed, this allows to prove the nonlinear stability of L_5 in the planar RTBP, for any $0 < \mu < \mu_R$, except for two values for which the point is unstable (see [32]). This leads to a region of perpetual stability of L_5 in the planar case, even though in the spatial case we can only talk about "effective stability" (i. e., stability for a very long time).

Due to the characteristic "banana shape" of the stability region, it is very useful to introduce the following adapted coordinates (see [12])

$$\begin{pmatrix} x \\ y \end{pmatrix} = \begin{pmatrix} \mu \\ 0 \end{pmatrix} + (1+\rho) \begin{pmatrix} \cos(2\pi\alpha) \\ \sin(2\pi\alpha) \end{pmatrix}, \tag{37}$$

to parametrize initial conditions, so that the point L_5 corresponds to $\alpha = 1/3$ and $\rho = 0$. An initial condition of the form

$$x_0 = x(\alpha, \rho), \quad y_0 = y(\alpha, \rho), \quad p_{x_0} = -y_0, \quad p_{y_0} = x_0 \tag{38}$$

is considered to be in the domain of stability of L_5 if it librates around the equilibrium point. This means that the trajectory does not approach to the primaries nor encircle the main one. A criteria to detect if a given trajectory escapes from L_5 is to check if it eventually satisfies $y < -0.5$ (see [13]). Note that the initial conditions of the form (38) have zero synodic velocity and do not belong to any particular energy manifold of H_0 (i. e., do not have the same Jacobi constant).

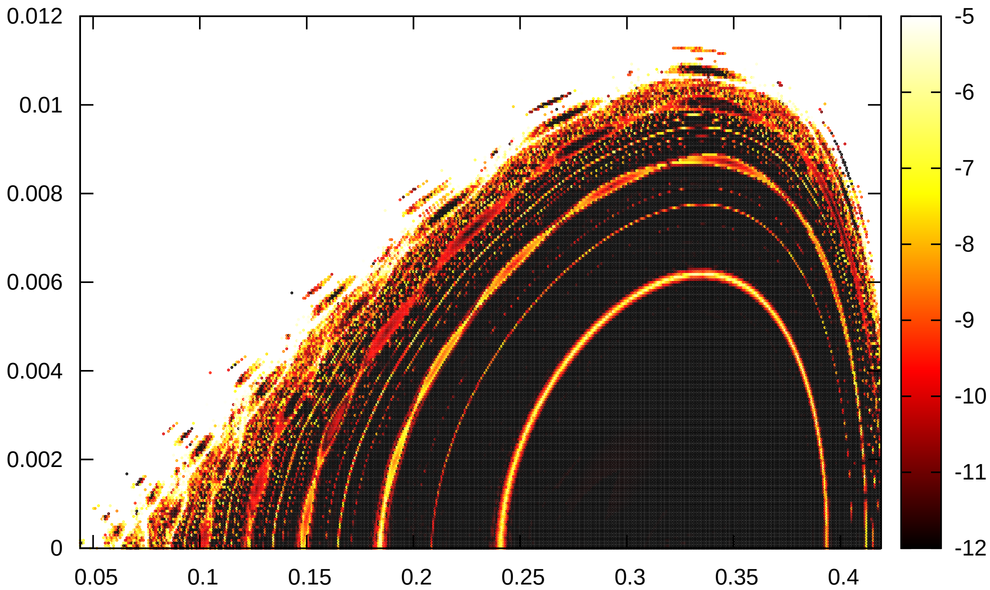

Figure 8: We plot ρ (vertical axis) versus α (horizontal axis) labelling the initial conditions (38) for the planar RTBP. We represent the error in the computation of the frequencies using a $\log_{10}$ color scale.

From the results reported in [12, 13], we know that the initial conditions in (38) that belong to the stability domain of L_5 are contained in the box $(\alpha, \rho) \in [0.03, 0.42] \times [-0.015, 0.015]$ and that this domain is symmetric with respect to $\rho = 0$. To perform a systematic computation of the basic frequencies of this problem, we take a grid 500×250 of values of (α, ρ) in this box and consider the corresponding initial conditions (38). For any initial condition, we introduce the complex signal $z_n = x(n) + \mathrm{i}y(n)$, defined by evaluating the trajectory of (34) at time $t = n \in \mathbb{N}$. Since we take the sampling time $T = 1$, we expect the computed frequencies for the discretized signal to give frequencies of the signal of continuous variable defined by the trajectory —assuming that we have a good enough approximation of them (see Remark 2.7). The numerical integration is performed using a Taylor method of order 24, working with double precision arithmetic and asking for local error 10^{-16}.

We are mainly interested in trajectories that belong to invariant tori with basic frequencies that are continuation of those of the elliptic point L_5. In analogy to a Lyapunov family of periodic orbits of an elliptic fixed point, we can refer to such tori as the (Cantor) family of Lagrangian invariant tori that emanates from L_5 (or simply to the family of invariant tori of L_5). We know that the set of initial conditions that belongs to a torus of this family has large relative Lebesgue measure if we are close enough to L_5 (see [9, 22]). Of course, it is clear that not any quasi-periodic solution in the region of stability of L_5 belongs to a torus of this family. For example, there are also "secondary invariant tori" created by the resonances, whose basic frequencies are not direct continuation of those of L_5 —incidentally, secondary tori also have "different topology" as do not turn around the point. Secondary tori are outside the scope of this systematic study.[5] There are other trajectories in the stability region of L_5 that are not quasi-periodic but, for example, have stochastic behaviour between the 2-dimensional tori confining them. As the initial approximations to the frequencies will be taken close to those of L_5, we expect the approach of the paper to fail for any trajectory not in the family that emanates from L_5 (even if it survives to the long time integration). Throughout the discussion we will abuse the notation introduced in (35), and we will refer to ω_1 and ω_2 as the frequencies of the family of invariant tori that emanates from L_5.

Initial approximations to the frequencies are obtained taking advantage of the fact that frequencies move very slowly with the initial conditions, so they remain very close to the planar frequencies (35) of the elliptic point (this is common to many problems in Celestial Mechanics). Specifically, we look for candidates in intervals of length 0.05 centered at the frequencies of L_5 (this length is suggested by the results reported in [12, 13]). Then, we evaluate the first $L = 1024$ iterates and, following Section 2.6, we compute $Z^{(1024,2)}(\omega_0)$ for 60 values of ω_0 in each of the two intervals, thus obtaining suitable candidates for the frequencies ω_1 and ω_2. This criteria has both a negligible computational cost and a good global performance for the range of orbits considered. Furthermore, we also use these iterates to compute simultaneously a rough approximation $\Gamma^{(0,2,10)}$ of the average of z_n, using the method in Section 2.5. Then, we redefine the signal by subtracting this estimated average, i. e., $z_n \mapsto z_n - \Gamma^{(0,2,10)}$. In this way we improve the performance of the unfolding procedure (see Remark 2.36).

Given an approximation of a frequency, we unfold the signal by applying the methodology of Section 2.3 with $p = 2$ (second order unfolding) and $q = 10$ (i. e., we use $L = 1024$ iterates to define any unfolded iterate). We refine the frequencies by the averaging-extrapolation method of Section 2.4, taking $p = 4$ and computing $2^{16} = 65536$ iterates of the signal at most. We stop the computations if two consecutive approximations to the frequencies differ less than 10^{-12}. If this tolerance is not reached along the integration, then we store the last values for the frequencies that we have computed as well as the estimated error. We observe that the maximum time that we integrate a trajectory is $t_{\max} = 2^{10} + 2^{16} = 66560$ (i. e., about 10593 revolutions of Jupiter). Of course, if during the integration we detect that the trajectory escapes (i. e., it satisfies $y < -0.5$), then the corresponding initial condition is rejected and we do not associate any frequency to it.

In the left plot of Figure 7 we show the points that have not been rejected. Of course, trajectories for these initial conditions can escape if $t_{\max}$ is increased. Note that due to the fact that KAM tori are sticky (see [33]), it is required to take a huge value of $t_{\max}$ in order to obtain a sharp estimation of the boundary of the domain of stability. For example, in the computations presented in [13], trajectories are integrated up to 200 Myears in physical time (about 16777216 revolutions of Jupiter). Characterizing this frontier of stability is not among the

[5] Besides the fact that to carry out the frequency analysis for a secondary torus we must perform a preliminary study of the signal in order to find a good set of approximate frequencies (see Section 2.6), we also have to be aware that (at least) one of the frequencies is small and with small amplitude.

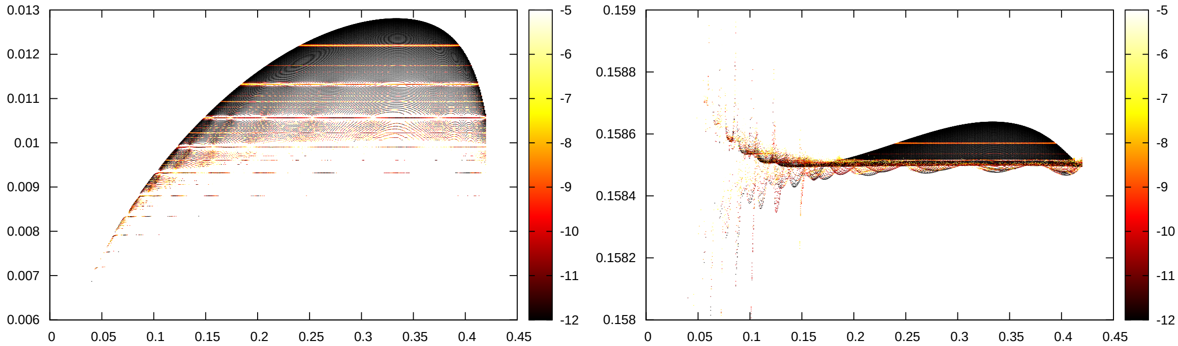

Figure 9: For the planar problem, we show $\omega_1/2\pi$ (left plot) and $\omega_2/2\pi$ (right plot) versus α for every ρ. We plot only those points with total error smaller than 10^{-5}.

aims of our approach. Nevertheless, it is worth paying attention to the behaviour of the method in this zone. Hence, we plot in black those points where the refinement of the frequency has a bad performance (specifically, when the sum of the final estimated errors for ω_1 and ω_2 is larger than $6 \cdot 10^{-6}$) and in red the remaining ones. If we compare with the domain of stability reported in [13, Figure 10], it seems that the black points are going to escape eventually (note that they accumulate at the boundary). Hence, the information given by the convergence of the method can allow us to detect some escaping trajectories before they leave the domain of influence of L_5, thus obtaining an approximation of the frontier of stability using a short range integration. We come back to this point later on.

In Figure 8 we plot the initial conditions (38) according to the convergence of the method. The palette of colors represents the sum of the final errors (in $\log_{10}$ scale) in the computation of ω_1 and ω_2 In account of the previous discussion, we select a color palette from white (error 10^{-5}) to black (error 10^{-12}). This palette is also used in subsequent figures. For a "good initial condition" (i. e., that belongs to a three dimensional invariant torus with frequencies close to those of L_5 and far from resonance), we require about 3000 Jupiter revolutions to reach the requested tolerance of 12 digits. In Figure 9 we show the computed frequencies $\omega_1/2\pi$ (left plot) and $\omega_2/2\pi$ (right plot) and the quotient ω_2/ω_1 is shown in Figure 10. As we mentioned, the frequencies present a small range of variation. We recall that we are asking the frequencies to be Diophantine (with a constant C in (2) not too small) in order to justify the validity of our averaging-extrapolation approach. Hence, it is not surprising that the convergence of the method has problems as we approach to a resonant zone and that the final error manifests this fact. Resonances correspond to $\omega_2/\omega_1 \in \mathbb{Q}$, and this color palette turns out to be very useful in order to visualize them (the integer ones and the semi-integer ones as well) in Figure 10. Another way to visualize this resonances is to fix a value of ρ and to plot the graph $\alpha \mapsto \omega_2/\omega_1$. This is done in the right plot of Figure 7 for $\rho = 0$. The result resembles a Devil's Staircase, which is a classical way to refer to the graph of the rotation number of a family of circle maps as a function of a parameter. Recall that a Devil's Staircase for a family of circle maps is a

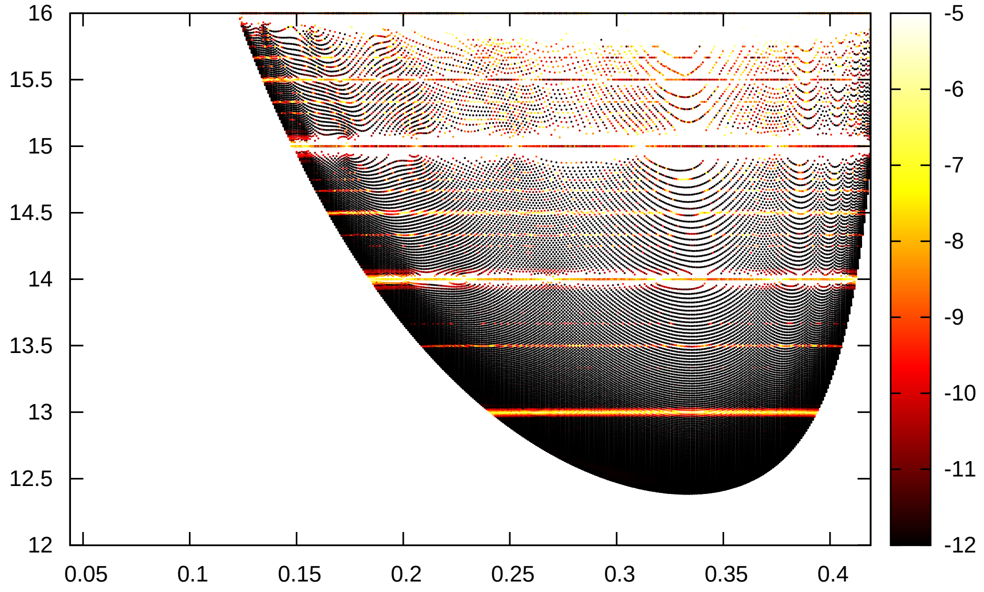

Figure 10: Computation of frequencies in the planar problem. We show ω_2/ω_1 versus α for every value of ρ. We restrict the figure to $\omega_2/\omega_1 \in [12, 16]$.

continuous graph but here we observe holes for the parameters for which there are no tori.

As it was discussed in Section 2.5 (see Remark 2.35), computing the amplitude corresponding to a given frequency is a very simple and reliable test to verify the computations performed. Although we rely on the fact that the refined frequencies remain close to the first approximation to validate the computations presented above, as follows we illustrate this test with a particular case. For example, let us consider the trajectory corresponding to $\alpha = 0.2211$ and $\rho = 0$, that has frequency

$$\omega_1/2\pi \simeq 0.011933549909.$$

We implement Proposition 2.32 to compute the amplitude corresponding to ω_1, taking $k^* = e_1 = (1, 0)$ and $p = 4$. Using $q = 15$, we obtain the approximation (clearly different from zero)

$$\hat{\gamma}_{e_1} \simeq \Gamma^{(e_1,4,15)} = 0.241593382 + 0.07606123\,\mathrm{i},$$

with an estimated error $3 \cdot 10^{-9}$.

Let us summarize some statistics of the obtained results. After integrating up to $t_{\max}$, we have that 54.8% of initial conditions escape from the region of libration around L_5. For 75.3% of the remaining trajectories, the total estimated error for the frequencies is smaller than 10^{-11}. We may consider that they belong to quasi-periodic invariant tori with (good) Diophantine frequencies. Only for 1.04% of the trajectories that do not escape, the frequencies have been approximated with an error larger than $5 \cdot 10^{-6}$. Many of these trajectories are close to the boundary of the region of stability and some of them will escape eventually after a larger integration. These numbers do not match exactly with the behaviour of the method reported in [13] since here we deal only with Lagrangian invariant tori of frequencies close to the ones of L_5. In [13] also secondary tori are taken into account.

Another phenomena that we want to illustrate is the effect of the sampling time T in the computation of the frequencies (see Remark 2.7). To this end, we consider a particular trajectory, given by $\alpha = 0.2952$ and $\rho = 0$, that has frequencies

$$\omega_1/2\pi \simeq 0.012689145311 \qquad \omega_2/2\pi \simeq 0.158623295518. \tag{39}$$

From this trajectory, we introduce quasi-periodic signals of the form $z_n = x(nT) + \mathrm{i}y(nT)$, $n \in \mathbb{N}$, for different sampling times $T \in (0, 4)$. Notice that after applying unfolding and refinement to compute a frequency $\bar{\omega}$ of the discretized signal in terms of the sampling time T, then we expect $\bar{\omega}/T$ to be a frequency of the original trajectory (at least for T not too large). We try to approximate ω_1 for different values of T according to the same implementation details used before. Indeed, a first approximation for the frequency is obtained from the study of $Z^{(2^{10},2)}(\omega_0)$. Then, to unfold the signal we use $p = 2$ and $L = 2^{10}$, and to compute the frequencies we use $p = 4$ and up to $N = 2^{14} = 16384$ iterates. The estimated error in the computation of ω_1 as a function of T is shown in the left plot of Figure 11. We observe that for small values of T the performance of the method improves when T increases. Beyond resonances, this phenomena is clear since the total integration time is proportional to T. This improvement stops when 14 correct digits have been obtained (we recall that computations are performed using double precision arithmetics). For largest values of T, the method behaves with less efficiency than expected when T is close to a resonant value of the form $T \approx 2\pi m/\langle \omega, k\rangle$, for some $k \in \mathbb{Z}^2$ and $m \in \mathbb{N}$ (see Remark 2.7). Some of the main resonances observed in the plot correspond to $m = 1$ and $k = (2, 2)$, $(1, 2)$, $(0, 2)$, $(-1, 2)$ and $(-2, 2)$. The value of T for these resonances are $T \simeq 2.918644$, 3.030893, 3.152122, 3.283453 and 3.426203.

Remark 3.3. *Note that since ω_1 is small, we only loss information on the frequency of the trajectory due to accumulated turns of the discretized signal if we take $T > 2\pi/\omega_1 \simeq 78.8$ (see Remark 2.7). In general, if we want to get rid of the effect of the accumulated turns due to the selection of T we can proceed as follows. Let us compute two numerical values $\omega^{(j)}$ for a frequency of the discretized signal —associated to the same approximate frequency of the trajectory— after considering two "unrelated" values of the sampling time, $T = T_j$, $j = 1, 2$. If we set $\widetilde{\omega}^{(j)} = \omega^{(j)}/T_j$, then a true value for the frequency of the trajectory can be identified by inspection of the coincidences between the sets $\{\omega^{(j)} + 2\pi m/T_j \,:\, m \in \mathbb{Z}^r\}$, for $j = 1, 2$.*

Following Section 2.4, we can compute frequencies with high accuracy due to the asymptotic behaviour $\mathcal{O}(1/N^{p+1})$ of the error. However, as the previous computations have been performed using double precision arithmetic, the maximum accuracy for the frequency is attained quickly and the results cannot be improved by considering more iterates nor higher extrapolation orders. We refer to [29, 30, 36] for detailed discussions in terms of computations performed

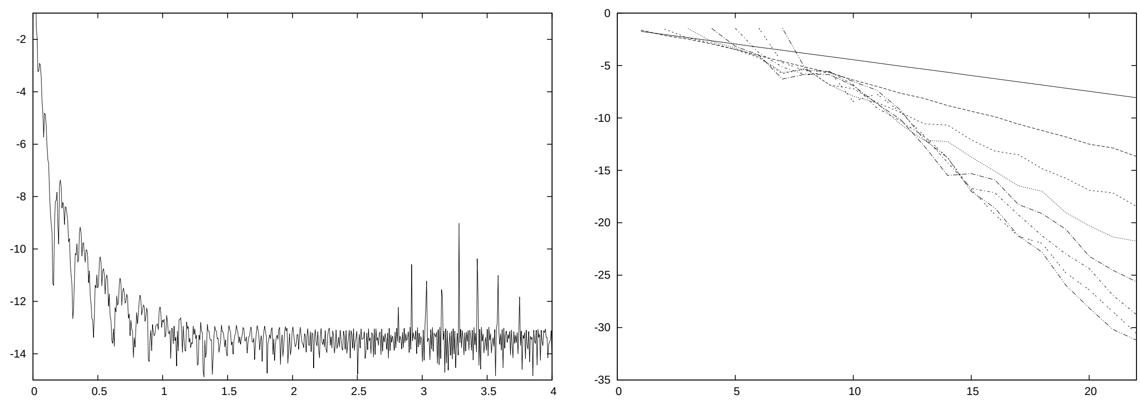

Figure 11: Left: Error (in $\log_{10}$ scale) versus the sampling time T in the computation of ω_1 in the planar problem for $\alpha = 0.2952$ and $\rho = 0$ (see (38)). Right: Error (in $\log_{10}$ scale) versus $q = \log_2 N$ in the computation of ω_1 for $\alpha = 0.2211$ and $\rho = 0$ for different extrapolation orders $p = 0, \ldots, 7$ (we joint consecutive points by lines).

using 32 and 64 digits arithmetics. To illustrate the behaviour of this methodology for large values of p and q, we present some computations performed using a 32 digits arithmetic. We integrate the vector field using a Taylor method of order 36 and asking for a tolerance of 10^{-32}. As an example, we tackle the computation of ω_1 for the trajectory given by $\alpha = 0.2211$ and $\rho = 0$. As sampling time we take $T = 1$ and as initial approximation of the frequency we take $\omega_1/2\pi \simeq 0.01193354991$ (the value we have previously obtained using double precision). As noted before, once the signal has been "successfully unfolded" (i. e., the wanted frequency is the one that leads the rotation of the projected signal), then the potential accuracy that we can reach for the frequency is not conditioned by the distance to a rigid rotation of the projected signal. In other words, improving the computation of the frequency by the averaging-extrapolation method of Section 2.4 does not require to increase the values $p = 2$ and $L = 2^{10}$ used to unfold the signal. Results are shown in the right plot of Figure 11. The vertical axis is the $\log_{10}$ of the error of the method, which gives (minus) the number of correct decimal digits (the error is estimated by comparing two consecutive computations). The horizontal axis means $q = \log_2 N$, where $N = 2^q$ is the number of iterates used to compute the frequency. The error-curves correspond to different values $p = 0, \ldots, 7$ of the extrapolation order (recall that if $p = 0$ then the method reduces to applying the definition of rotation number). As expected, for $N = 2^{22}$ the curve are ordered from top to bottom by increasing value of the extrapolation order p. One can check that, for a sufficiently large value of q, the slope of the curves tends to be $-(p+1)\log_{10} 2$, as expected due to the asymptotic behaviour of the error.

As observed in Remark 2.36, the computation of the average of the discretized signal is a simple (and fast) indicator to detect candidates to quasi-periodic solutions (without computing any frequency). To show the features of this approach, we take a grid 500×250 of initial values of $(\alpha, \rho) \in [0.08, 0.15] \times [0.0025, 0.0065]$. This corresponds to a zoom of the left plot of Figure 7 and of Figure 8, that contains part of the boundary of the domain of stability (see the marked

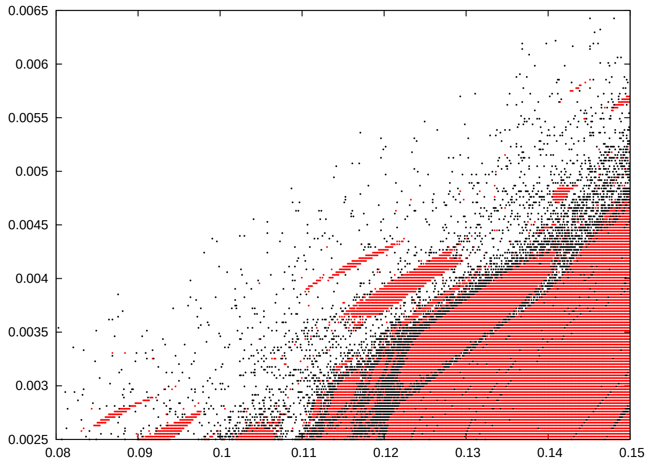

Figure 12: We plot ρ versus α for the points inside the marked rectangle of Figure 7. We use white for those conditions that escape before $t_{\max} = 8192$, black for those points where the final estimated error in the computation of the average is larger than 10^{-4} after $t_{\max}$, and red otherwise.

rectangle in Figure 7). Then, we use the algorithm described in Proposition 2.32 to compute the average of the corresponding trajectories. Specifically, we take $p = 4$ and $2^{13} = 8192$ iterates at most in formula (30), with sampling time $T = 1$. As we only want to detect such trajectories for which the average seems to converge, but not an accurate value for it, we stop the computations if the difference between two consecutive iterations, i. e., $|\Gamma^{(0,4,q)} - \Gamma^{(0,4,q-1)}|$, is less than 10^{-8}. In Figure 12 we show the points that have not been rejected after $t_{\max} = 8192$. We plot in black those points where the computation of the average has a bad performance (the final estimated error is larger than 10^{-4}) and in red the remaining ones.

Notice that looking at the red points we obtain a nice approximation of the boundary of stability using a relatively short integration time, only about 1304 Jupiter revolutions at most. Compare with the 16777216 revolutions (at most) used in [13] to accurately characterize the boundary in terms of the criteria that escaping solutions eventually reach $y < -0.5$. In other words, we note that many points which will eventually escape after a long integration are still librating around L_5 after the considered integration time, but the accuracy of the average is less than 10^{-4}. We emphasize that computing the average is useful for detecting initial conditions that belong to secondary tori. However, it has the inconvenient that some of these “bad” points correspond to trajectories confined inside the domain of stability, but that do not belong to any invariant torus of the system.

Although to analyze the behaviour of the computation of the average by averaging and extrapolation is not the purpose of this work, we think that this approach is interesting in order to study a wide set of problems in a systematic way —to detect either escaping or chaotic trajectories, since computing the average can be done with high accuracy at a very low computational cost. Moreover, this has the advantage of being a general criteria, independent of the problem

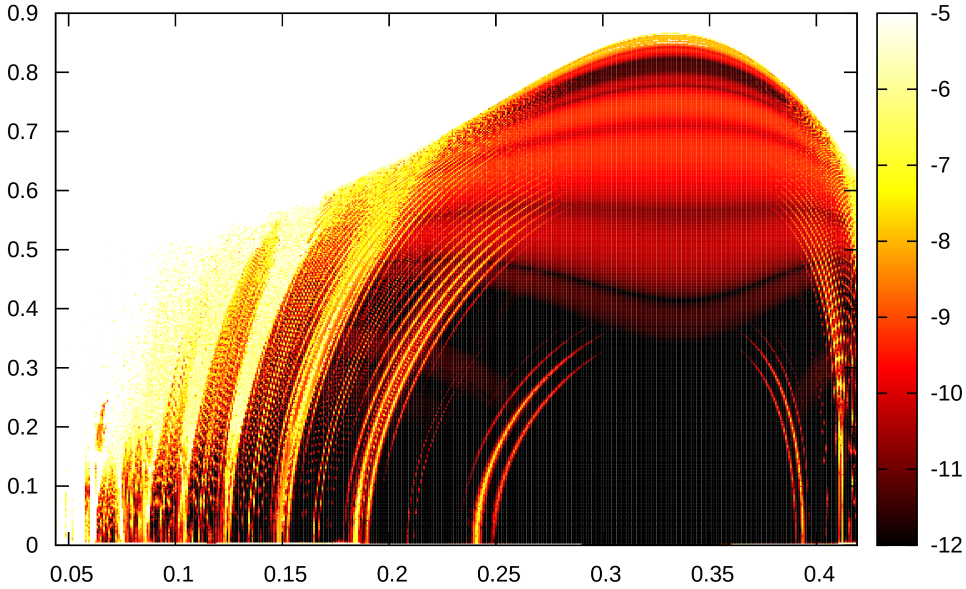

Figure 13: We plot z (vertical axis) versus α (horizontal axis) labelling the initial conditions in the spatial problem according to (41). We represent the error in the computation of the three basic frequencies using a $\log_{10}$ color scale.

at hand (we do not require particular characterizations of escaping orbits such us the criteria $y < -0.5$).

3.2 Spatial case

Now we consider the full Hamiltonian (34). In the spatial RTBP we cannot properly speak about the stability domain of L_5, as the 3-dimensional KAM tori of the system do not act as barriers for the solutions in the 5-dimensional energy manifolds. Hence, beyond the set of positive Lebesgue measure defined by these invariant tori, for a general trajectory of the spatial RTBP we can only ask for effective stability (i. e., stability for long time, in the aim of the classical Nekhoroshev estimates).

In this case, it is know that the extension to $z > 0$ of the domain of stability of L_5 has a paraboloid shape. Then, a good parametrization for the initial conditions is the following (we refer to [39])

$$\begin{pmatrix} x \\ y \\ z \end{pmatrix} = \begin{pmatrix} \mu \\ 0 \\ z \end{pmatrix} + (1 + \rho - \sqrt{\psi(z^2)}) \begin{pmatrix} \cos(2\pi\alpha) \\ \sin(2\pi\alpha) \\ 0 \end{pmatrix}, \tag{40}$$

where

$$\psi(w) = 1 - \frac{1}{2}w + \frac{3}{2^5}w^2 - \frac{1}{2^8}w^3 - \frac{25}{2^{13}}w^4 + \frac{33}{2^{16}}w^5 + \frac{175}{2^{20}}w^6 - \frac{497}{2^{23}}w^7 - \frac{4401}{2^{29}}w^8 + \cdots .$$

We fix $\rho = 0$ and we take a grid 500×500 of values of $(\alpha, z) \in [0.03, 0.42] \times [0, 1]$. Then, we take initial conditions with zero synodic velocity parametrized as

$$x_0 = x(\alpha, 0, z), \quad y_0 = y(\alpha, 0, z), \quad z_0 = z, \quad p_{x_0} = -y_0, \quad p_{y_0} = x_0, \quad p_{z_0} = 0. \qquad (41)$$

For any of these trajectories we introduce the complex signal $z_n = x(n) + \mathrm{i}y(n)$, by taking again sampling time $T = 1$.

We compute the frequencies ω_1, ω_2 and ω_3 of the invariant tori emanating from the point L_5. Implementation parameters are very similar to those used in the planar case (see Section 3.1). The numerical integration is performed using a Taylor method of order 24, working with double precision arithmetic and asking for local error 10^{-16}. Initial approximations to the basic frequencies are obtained starting from the information of the planar problem. Hence, for $z \simeq 0$, to approximate ω_1 and ω_2 we look for peaks close to the frequencies computed for the planar case and to approximate ω_3 for a peak close to 1. After this triplet of frequencies has been refined, we increase the value of z, and we use the previously obtained frequencies as a reference values to look for candidates (peaks) for the new ones. We look for peaks in intervals of length 0.0032 around each of these reference values, by computing $Z^{(1024,2)}(\omega_0)$ (see Section 2.6) for 60 values of ω_0 in any of the three intervals. It is worth mentioning that ω_2 is so close to ω_3 such that we have to pay attention to this fact to guarantee that we have a good approximation of any of them. Otherwise, combination of unfolding and refinement converges to the same result for the two approximations.

As in the planar case, we use the method in Section 2.5 to compute a rough approximation of the average of the signal, and we redefine z_n by subtracting this average. Specifically, we introduce $z_n \mapsto z_n - \Gamma^{(0,2,10)}$. Then, we unfold the signal by applying the methodology of Section 2.3, with $p = 2$ (second order unfolding) and $q = 10$ (i. e., we use $L = 1024$ iterates to define any unfolded iterate). We refine the frequencies by the averaging-extrapolation method of Section 2.4, taking $p = 4$ and computing $2^{16} = 65536$ iterates of the signal at most. We stop the computations if two consecutive approximations to the frequencies differ less than 10^{-12}.

In Figure 13 we plot the considered initial conditions (41) colored according to the convergence of the method. The palette of colors represents the sum of the estimated errors (in $\log_{10}$ scale) in the approximation of the three frequencies. Let us observe that set of points where the computation of the frequencies is not performed accurately correspond to the "geometrical continuation" to $z > 0$ of the resonances observed in Figure 8 for $\rho = 0$. We have repeated the computations for initial conditions defined as in (41), but for different values of ρ in (40), obtaining analogous results.

In Figure 14 we represent some combinations of the frequencies associated to the points in Figure 13. We plot a zoom to enhance the structure of the plot. We use the same $\log_{10}$

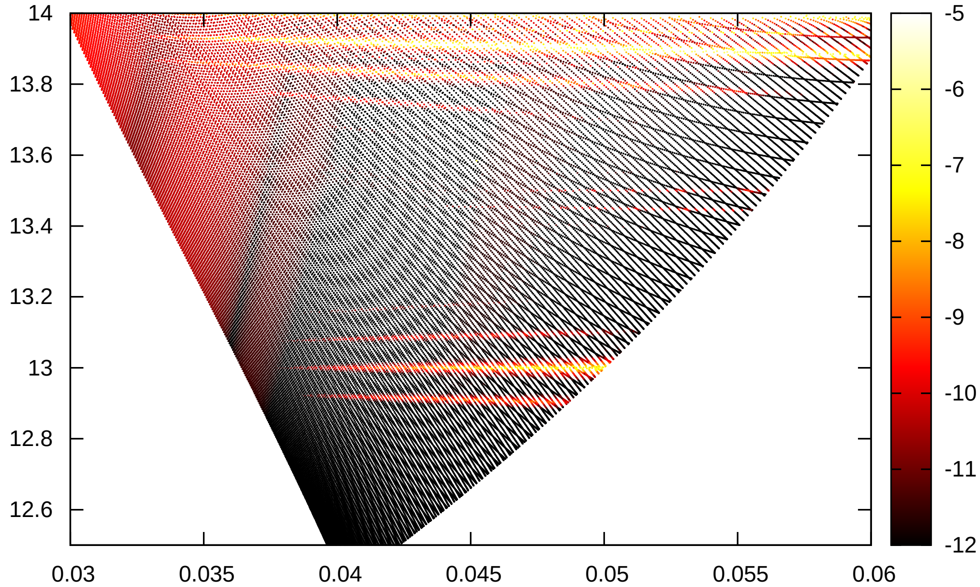

Figure 14: Left: We plot the quotients ω_2/ω_1 (vertical axis) versus $(\omega_3 - \omega_2)/\omega_1$ (horizontal axis) for a zoom of the selected grid of conditions in the spatial problem according to (41). We use the same color palette for the error as in Figure 13.

color palette for the error as in Figure 13 in order to visualize the main resonances. Note that resonances correspond to vanishing integer combinations of the three frequencies. As ω_2 and ω_3 are very close, we select to show ω_2/ω_1 versus $(\omega_3 - \omega_2)/\omega_1$, so that resonances correspond to lines with equations having integer coefficients. Apart from the resonances, we observe that in the plot the points look as if they were distributed in curves. A natural explanation is that the map

$$(\alpha, z) \longmapsto \left(\frac{\omega_3 - \omega_2}{\omega_1}, \frac{\omega_2}{\omega_1} \right)$$

behaves as a diffeomorphism on a Cantor-like set of large Lebesgue measure. Hence, as we plot the points corresponding to the grid of values of (α, z) by moving through coordinate lines, then we observe the image of these lines as smooth curves.

Finally, we present some statistics of the obtained results. We obtain that 61.18% of the trajectories do not escape after integrating up to $t_{\max}$. For 2.17% of these trajectories, the sum of the (estimated) errors in the computation of the three frequencies is larger than $5 \cdot 10^{-6}$. We expect most of them to escape after a longer (possibly large) integration. For 45.45% of them, the sum of the errors is smaller than 10^{-11}. We hope that these trajectories belong to quasi-periodic invariant tori whose basic frequencies are “very” Diophantine and close to the normal ones of L_5.

Planet	$\hat{\omega}_i$	m_i	a_i
Neptune	0.92801432138537394	5.1464752074960787e-5	5.7788760748791814
Saturn	0.59716051258412511	2.8561327940941584e-4	1.8335242195766197
Uranus	0.85880670883551138	4.3620791653297386e-5	3.6880511883932363
Earth	-0.1862408594090464	3.0375324347911519e-6	0.1923832582416737

Table 1: Frequencies, masses and radii of the planets used in (36).

q	$\hat{\omega}_1$	$\hat{\omega}_2$
5	0.928653980143709743165276669468929	0.599382329537292660651851066335658
6	0.928074698141400367886405365621802	0.597353799463132731867813521970719
7	0.928011406040210073007649328662823	0.597170683287294613337166912438880
8	0.928012981190058882970132062540001	0.597160863433890478048734042323353
9	0.928014783293092087664994619614988	0.597160521394420061323830787193378
10	0.928014660962250750396756626759760	0.597160512759816035323654200831792
11	0.928014284064984417486857651312489	0.597160512587858793607019746153710
12	0.928014321724697792320504173605765	0.597160512584175033828001053659716
13	0.928014321376624582553768362236468	0.597160512584126112117500504427987
14	0.928014321385749303967589813025608	0.597160512584125119156675196553359
15	0.928014321385373754789964541932186	0.597160512584125110225098552299600
16	0.928014321385373872422970145789419	0.597160512584125110004368874099029
17	0.928014321385373941447437305728162	0.597160512584125110000035659584528
18	0.928014321385373940000194018750186	0.597160512584125110000000852394702
19	0.928014321385373939999739724886880	0.597160512584125110000000016821083
20	0.928014321385373940000004910137652	0.597160512584125110000000000142700

Table 2: Computed frequencies of the torus that replaces the point L_5 in presence of Saturn and Neptune for different values of $q = \log_2 N$.

3.3 Multicircular problem

Now we consider the Hamiltonian (36), where the effect of additional planets, according to the so-called multicircular problem, is taken into account (see Table 1). Specifically, we consider the effect of Saturn, Uranus, Neptune and Earth, being the fist one the most significant perturbation. This model was studied in [20], where the 4-dimensional invariant torus that replaces the point L_5 was computed. Note that we expect the invariant tori of the autonomous spatial system to enlarge their dimension by adding the frequencies of the planets (see [23, 38]). Indeed, the natural quasi-periodic solutions of (36) have 7 basic frequencies, even though 4 of them are known a priori. Here we use the methodology introduced in this paper to analyze the abundance of quasi-periodic solutions around the point L_5 (indeed, around the 4-dimensional torus that replaces it) by computing the remaining 3 basic frequencies (as a continuation of the normal ones of L_5) for the stable solutions. Note that we keep the notation ω_1, ω_2 and ω_3 for the continuation of the frequencies of L_5 and we denote by $\hat{\omega}_1$, $\hat{\omega}_2$, $\hat{\omega}_3$ and $\hat{\omega}_4$ the frequencies of the forcing.

We take the same initial conditions (41) as in Section 3.2, using the same grid of values of

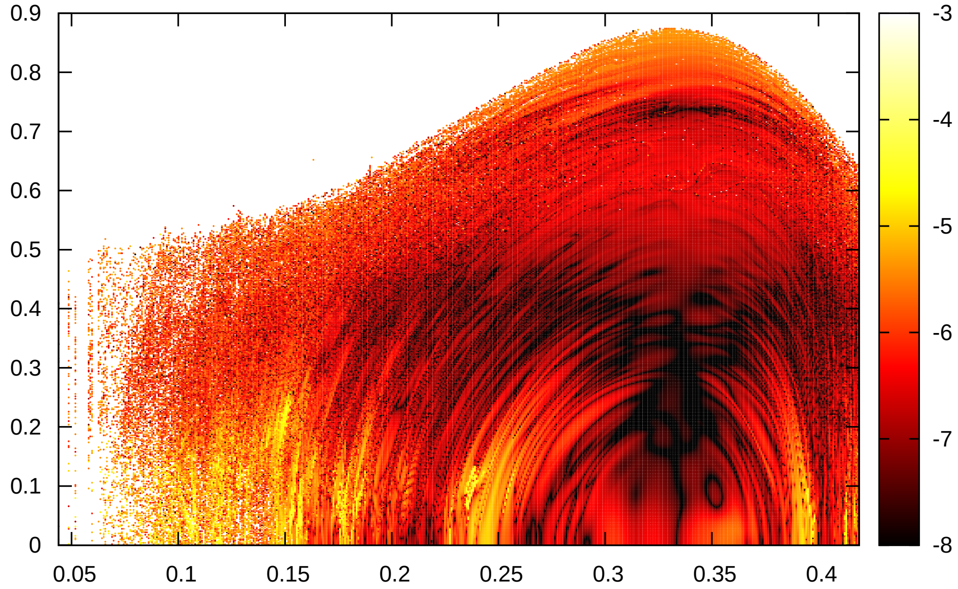

Figure 15: We plot z (vertical axis) versus α (horizontal axis) labelling the initial conditions in the Multicircular problem according to (41). We represent the error in the computation of the three basic frequencies using a $\log_{10}$ color scale.

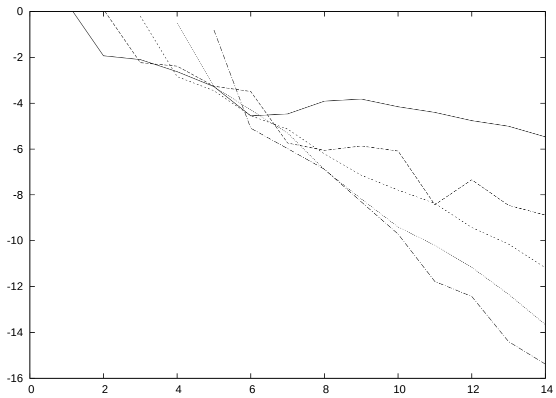

Figure 16: Study of the torus that replaces the point L_5 in presence of Saturn and Neptune. We plot the error (in $\log_{10}$ scale) versus $q = \log_2 N$, for different values of p, corresponding to the computation of the average.

(α, z) to parametrize (40), and we define the complex signal $z_n = x(n) + \mathrm{i}y(n)$ by integrating (36). The implementation details are also the same as in Section 3.2, including the strategy for computing initial approximations to the frequencies by performing continuation with respect to z. However, since the numerical integration of this problem is computationally more demanding than the spatial RTBP, we restrict the maximum number of iterates to $2^{14} = 16384$

(about 2607 Jupiter revolutions) and we stop the computations if two consecutive approximations to the frequencies differ less than 10^{-8}. Nevertheless, from the qualitative point of view, the obtained results look similar to those for larger integration times.

Results are shown in Figure 15. As done before, we use a $\log_{10}$ color palette to represent initial conditions according to the performance of the method. Comparing with Figure 13, we observe that the quasi-periodic perturbation produces significant changes in the region of stability around the torus replacing L_5. Indeed, the size of the domain of effective stability remains essentially the same, but a larger quantity of invariant tori of the RTBP are destroyed by the perturbation, specially in the horizontal direction. In particular, we find quasi-periodic solutions in a region that is above (in the vertical direction) the torus that replaces L_5. This is consistent with the fact that this torus is linearly stable. Further, this is also in accordance with the study presented in [19] for the Bicircular problem Earth-Moon-Sun, in which the periodic orbit replacing L_5 turns unstable, even though stable motion are still obtained in the vertical direction (of course the effect of Saturn in the Sun-Jupiter case is not as dramatic as the effect of Sun in the Earth-Moon case).

As far as statistics is concerned, we have that 59.57% of the trajectories have not escaped after integrating up to $t_{\max}$. This number is slightly smaller than for the spatial RTBP ("the unperturbed problem"), but in this case $t_{\max}$ is significantly smaller. In fact, comparing with the RTBP, we expect a larger amount of trajectories to escape for large values of $t_{\max}$. In addition, only 4.56% of the points that have not escaped present an estimated error for the three frequencies smaller that 10^{-7}. Recall that we are integrating at most up to $t_{\max} = 16384$ and we can obtain higher precision for the frequencies by taking a larger integration time.

Next, we study the frequencies of a particular orbit using a larger number of iterates. For this reason, we select an initial condition that is known to be on an invariant torus. Specifically, we consider the 2-dimensional torus that replaces L_5 in presence of Saturn and Neptune. This torus, that has as basic frequencies $\hat{\omega}_1$ and $\hat{\omega}_2$ (those of Saturn and Neptune), has been numerically computed in [20, see bottom plot of Figure 5], and it is characterized by the initial condition

$$x = -0.49507899400971284, \quad y = 0.86774513932356423, \quad z = \dot{x} = \dot{y} = \dot{z} = 0. \tag{42}$$

We consider first the computation of the average $\hat{\gamma}_0 \simeq \Gamma^{(0,p,q)}$ (see Proposition 2.32) of this quasi-periodic trajectory. The numerical integration is performed using a Taylor method of order 24 working with double precision arithmetic and asking for local error 10^{-16}. In Figure 16, we show the log_{10} of the estimated error $|\Gamma^{(0,p,q)} - \Gamma^{(0,p,q-1)}|$ versus $q = \log_2 N$, for different values of the averaging order p. As expected, the behaviour is analogous to Figure 11. Note that if we take $p = 4$ and $q = 14$, we approximate the average almost with double precision.

Finally, we face the computation of frequencies $\hat{\omega}_1$ and $\hat{\omega}_2$ from the discretized trajectory of (42) by unfolding, averaging and extrapolation. Although these frequencies are already known, we want to show that its computation can be carried out with high precision by the approach of the paper. We want to emphasize, that as we are dealing with frequencies coming from a "small" quasi-periodic perturbation, the effectiveness of the unfolding approach for its computation is not secured a priori (see Remark 2.14). Computations are performed using an arithmetic of 32 decimal digits. The numerical integration is performed using a Taylor method of order 36, asking for a tolerance of 10^{-32}. Although we could use the values in Table 1 as "approximations" to the frequencies for the unfolding, we act as if they are unknown and we look for candidates for the frequencies looking for peaks in the intervals $[0.88, 0.95] \ni \hat{\omega}_1$ and $[0.56, 0.64] \ni \hat{\omega}_2$. Specifically, we use the criteria described in Section 2.6, computing $Z^{(1024,2)}(\omega_0)$ for 60 values of ω_0 in each interval. As before, to improve the performance of the unfolding procedure, we redefine the signal by subtracting a (rough) approximation of its average, i. e., $z_n \mapsto z_n - \Gamma^{(0,2,10)}$ (see Remark 2.36). To unfold the signal we use $p = 2$ and $L = 1024$. To refine the frequencies of Saturn and Neptune, we use $p = 5$ and compute up to $N = 2^{20}$ iterates of the unfolded signal. In Table 2, we present the approximation of both frequencies for different values of $q = 5, \ldots 20$, where 2^q is the number of iterates of the unfolded signal. Notice that the method performs very well in high precision and we obtain the digit 0 beyond the truncated precision of the initial data.

4 Conclusions and final remarks

In this paper we have presented a methodology to perform frequency analysis of analytic quasi-periodic signals with Diophantine basic frequencies. Given a good approximation of any of the frequencies, we can refine it up to high precision at a moderate computational cost and low memory requirements. The method is very flexible and self-contained, in the sense that it also allows us to obtain initial approximations of the frequencies when we have no previous information on them. Such initial approximations are more accurate than the ones obtained by straight use of DFT.

A remarkable feature of our approach it that refining a particular frequency does not require any information on the other frequencies neither to compute simultaneously any Fourier coefficient of the signal. The accuracy of the method is not constrained by the number of significant Fourier harmonics required to approximate the quasi-periodic signal nor by the dimension of the vector of basic frequencies of the problem. Fourier coefficients can be obtained a posteriori, by slightly modifying the procedure for calculating the frequencies.

Among the strengths of our approach, we mention that it is dynamically coherent with the problem. Indeed, algorithms preserve the quasi-periodic structure of the original signal. No spurious frequencies are added due to the truncation of the signal to a finite sample and it is not necessary to turn the signal into a periodic one in order to magnify its dominant frequencies. We also want to highlight that the presented algorithms are extremely simple to code and optimize.

Specifically, the largest set of data required to store in memory is an array of length L, that corresponds to the number of iterates used to define an iterate of the unfolded signal. The time cost of computing an unfolded iterate is essentially the cost of evaluating an iterate of the original signal and performing $4p_u$ products (see Remark 2.23), where p_u is the order of the unfolding. The computational cost of a frequency refinement of order p_r, using N iterates of the unfolded signal, is essentially the cost of evaluating N unfolded iterates and performing $2p_r$ products. There are several parameters to optimize for a given particular problem (sampling time, averaging orders, etc.). In this paper we do not present a close criteria to optimize them, since it depends on several factors such as the computational cost of evaluating the signal, the magnitude of the Fourier coefficients related to the frequencies to be computed or the precision required in the results.

The main limitations of the method are the case of signal with poor regularity and the computation of frequencies close to resonance or that barely contribute to the signal (i. e., with very small amplitude). Comparison with other methods must take into account the computational cost of the iterates, because high accuracy may require a large number of them. Indeed, if we want to compute frequencies up to a very high accuracy, then it is reasonable to use an arithmetic with a large number of decimal digits which, of course, increases significantly the computational cost of any iterate. As mentioned above, our approach also allows us to compute the amplitudes of the signal. However, if many amplitudes are required, then the use of collocation methods is most probably a better choice.

Finally, we want to emphasize that the "inverse problem" to the frequency analysis can also be tackled with the same ideas of the paper. Given a fixed $\omega \in \mathbb{R}^d$, it consists in computing an initial condition for an invariant torus of a Hamiltonian system with d degrees of freedom, or for a symplectic map in $\mathbb{R}^{2d}$, having ω as a vector of basic frequencies. Of course, ω must be Diophantine and we require to know a good enough approximation to this initial condition (assuming that the torus exists). The keystone is to combine the methodology of the paper for the frequency analysis (note that ω is the approximate frequency we use for the unfolding) with the computation of derivatives of frequencies with respect to parameters and initial conditions already introduced in [29]. This information allows us to refine the approximation for this initial condition by applying the Newton method to the d-dimensional frequency map. Note that the frequency map is well defined in a small neighbourhood of a Diophantine torus —except for a set of exponentially small Lebesgue measure in the distance to the torus— and has $\mathcal{C}^\infty$-Whitney regularity. This problem is postponed to future work.

Acknowledgements

We wish to thank comments, suggestions and fruitful discussions with Luis Benet, Àngel Jorba, Rafael de la Llave and Carles Simó. We also thank À. Jorba for providing us the initial condition (42).

References

[1] V.I. Arnold. Proof of a theorem of A. N. Kolmogorov on the invariance of quasi-periodic motions under small perturbations. *Russian Math. Surveys*, 18(5):9–36, 1963.

[2] R. Barrio. Performance of the Taylor series method for ODEs/DAEs. *Appl. Math. Comput.*, 163(2):525–545, 2005.

[3] H.W. Broer, G.B. Huitema, and M.B. Sevryuk. *Quasi-periodic motions in families of dynamical systems. Order amidst chaos*. Lecture Notes in Math., Vol 1645. Springer-Verlag, Berlin, 1996.

[4] H.W. Broer and M.B. Sevryuk. KAM theory: Quasi-periodicity in dynamical systems. In *Handbook of Dynamical Systems*, volume 3C, pages 249–344. Elsevier, 2010.

[5] A. Celletti and A. Giorgilli. On the stability of the Lagrangian points in the spatial restricted problem of three bodies. *Celestial Mech. Dynam. Astronom.*, 50(1):31–58, 1991.

[6] R. de la Llave. A tutorial on KAM theory. In *Smooth ergodic theory and its applications (Seattle, WA, 1999)*, volume 69 of *Proc. Sympos. Pure Math.*, pages 175–292. Amer. Math. Soc., Providence, RI, 2001.

[7] R. de la Llave, A. González, À. Jorba, and J. Villanueva. KAM theory without action-angle variables. *Nonlinearity*, 18(2):855–895, 2005.

[8] R. de la Llave and A. Luque. Differentiability at the tip of Arnold tongues for Diophantine rotations: numerical studies and renormalization group explanations. *J. Stat. Phys.*, 143(6):1154–1188, 2011.

[9] A. Delshams and P. Gutiérrez. Estimates on invariant tori near an elliptic equilibrium point of a Hamiltonian system. *J. Differential Equations*, 131(2):277–303, 1996.

[10] L.H. Eliasson. Perturbations of stable invariant tori for Hamiltonian systems. *Ann. Scuola Norm. Sup. Pisa Cl. Sci. (4)*, 15(1):115–147 (1989), 1988.

[11] A. Giorgilli, A. Delshams, E. Fontich, L. Galgani, and C. Simó. Effective stability for a Hamiltonian system near an elliptic equilibrium point, with an application to the restricted three-body problem. *J. Differential Equations*, 77(1):167–198, 1989.

[12] G. Gómez, À. Jorba, C. Simó, and J. Masdemont. *Dynamics and mission design near libration points. Vol. IV. Advanced methods for triangular points*, volume 5 of *World Scientific Monograph Series in Mathematics*. World Scientific Publishing Co. Inc., River Edge, NJ, 2001.

[13] G. Gómez, J.-M. Mondelo, and C. Simó. A collocation method for the numerical Fourier analysis of quasi-periodic functions. I. Numerical tests and examples. *Discrete Contin. Dyn. Syst. Ser. B*, 14(1):41–74, 2010.

[14] G. Gómez, J.-M. Mondelo, and C. Simó. A collocation method for the numerical Fourier analysis of quasi-periodic functions. II. Analytical error estimates. *Discrete Contin. Dyn. Syst. Ser. B*, 14(1):75–109, 2010.

[15] A. González, R. de la Llave, and A. Haro. Singularity theory for non-twist KAM tori. To appear in Memoirs of the AMS.

[16] M.R. Herman. Une méthode pour minorer les exposants de Lyapounov et quelques exemples montrant le caractère local d'un théorème d'Arnol'd et de Moser sur le tore de dimension 2. *Comment. Math. Helv.*, 58(3):453–502, 1983.

[17] T.H. Jäger and J. Stark. Towards a classification for quasiperiodically forced circle homeomorphisms. *J. London Math. Soc. (2)*, 73(3):727–744, 2006.

[18] W.B. Jones and V. Petersen. Continued fractions and Szegő polynomials in frequency analysis and related topics. In *Proceedings of the International Conference on Rational Approximation, ICRA99 (Antwerp)*, volume 61, pages 149–174, 2000.

[19] À. Jorba. A numerical study on the existence of stable motions near the triangular points of the real earth-moon system. *Astronomy and Astrophysics*, 364:327–338, 2000.

[20] À. Jorba and E. Olmedo. On the Computation of Reducible Invariant Tori on a Parallel Computer. *SIAM J. Appl. Dyn. Syst.*, 8(4):1382–1404, 2009.

[21] À. Jorba, R. Ramírez-Ros, and J. Villanueva. Effective reducibility of quasi-periodic linear equations close to constant coefficients. *SIAM J. Math. Anal.*, 28(1):178–188, 1997.

[22] À. Jorba and J. Villanueva. On the normal behaviour of partially elliptic lower-dimensional tori of Hamiltonian systems. *Nonlinearity*, 10(4):783–822, 1997.

[23] À. Jorba and J. Villanueva. On the persistence of lower-dimensional invariant tori under quasi-periodic perturbations. *J. Nonlinear Sci.*, 7(5):427–473, 1997.

[24] À. Jorba and M. Zou. A software package for the numerical integration of ODEs by means of high-order Taylor methods. *Experiment. Math.*, 14(1):99–117, 2005.

[25] J. Laskar. The chaotic motion of the solar system. A numerical estimate of the size of the chaotic zones. *Icarus*, 88:266–291, 1990.

[26] J. Laskar. Introduction to frequency map analysis. In *Hamiltonian systems with three or more degrees of freedom (S'Agaró, 1995)*, volume 533 of *NATO Adv. Sci. Inst. Ser. C Math. Phys. Sci.*, pages 134–150. Kluwer Acad. Publ., Dordrecht, 1999.

[27] J. Laskar. Frequency map analysis and quasiperiodic decompositions. In *Hamiltonian systems and Fourier analysis*, Adv. Astron. Astrophys., pages 99–133. Camb. Sci. Publ., Cambridge, 2005.

[28] J. Laskar, C. Froeschlé, and A. Celletti. The measure of chaos by the numerical analysis of the fundamental frequencies. Application to the standard mapping. *Phys. D*, 56(2-3):253–269, 1992.

[29] A. Luque and J. Villanueva. Computation of derivatives of the rotation number for parametric families of circle diffeomorphisms. *Phys. D*, 237(20):2599–2615, 2008.

[30] A. Luque and J Villanueva. Numerical computation of rotation numbers for quasi-periodic planar curves. *Phys. D*, 238(20):2025–2044, 2009.

[31] A. Luque and J. Villanueva. A KAM theorem without action-angle variables for elliptic lower dimensional tori. *Nonlinearity*, 24(4):1033–1080, 2011.

[32] A.P. Markeev. On the stability of the triangular libration points in the circular bounded three-body problem. *J. Appl. Math. Mech.*, 33:105–110, 1969.

[33] A.D. Perry and S. Wiggins. KAM tori are very sticky: rigorous lower bounds on the time to move away from an invariant Lagrangian torus with linear flow. *Phys. D*, 71(1-2):102–121, 1994.

[34] McKenzie R. and Szebehely V. Non-linear stability motion around the triangular libration points. *Celestial Mechanics*, 23:223–229, 1981.

[35] P. Robutel, F. Gabern, and A. Jorba. The observed Trojans and the global dynamics around the Lagrangian points of the Sun-Jupiter system. *Celestial Mech. Dynam. Astronom.*, 92(1-3):53–69, 2005.

[36] T.M. Seara and J. Villanueva. On the numerical computation of Diophantine rotation numbers of analytic circle maps. *Phys. D*, 217(2):107–120, 2006.

[37] T.M. Seara and J. Villanueva. Numerical computation of the asymptotic size of the rotation domain for the Arnold family. *Phys. D*, 238(2):197–208, 2009.

[38] M.B. Sevryuk. Invariant tori in quasi-periodic non-autonomous dynamical systems via Herman's method. *Discrete Contin. Dyn. Syst.*, 18(2-3):569–595, 2007.

[39] C. Simó, P. Sousa-Silva, and M. Terra. Domains of Practical Stability near $l_{4,5}$ in the 3D Restricted Three-Body Problem. In preparation, 2012.

[40] V. Szebehely. *Theory of Orbits — The Restricted Problem of Three Bodies*. Academic Press, New York, 1967.

[41] L.V. Vela-Arevalo and J.E. Marsden. Time-frequency analysis of the restricted three-body problem: transport and resonance transitions. *Classical Quantum Gravity*, 21(3):S351–S375, 2004. A spacetime safari: essays in honour of Vincent Moncrief.